DISSERTATION

ELECTRON-REFLECTOR STRATEGY FOR CdTe THIN-FILM SOLAR CELLS

Submitted by

Kuo-Jui Hsiao

Department of Physics

In partial fulfillment of the requirements

For the Degree of Doctor of Philosophy

Colorado State University

Fort Collins, Colorado

Spring 2010

COLORADO STATE UNIVERSITY

April 2, 2010

WE HEREBY RECOMMEND THAT THE DISSERTATION PREPARED UNDER OUR SUPERVISION BY KUO-JUI HSIAO ENTITLED ELECTRON-REFLECTOR STRATEGY FOR CdTe THIN-FILM SOLAR CELLS BE ACCEPTED AS FULFILLING IN PART REQUIREMENTS FOR THE DEGREE OF DOCTOR OF PHILOSOPHY.

Committee on Graduate Work

_____
Martin Gelfand

_____
Robert Leisure

_____
Walajabad Sampath

_____
Advisor: James Sites

_____
Department Head: Dieter Hochheimer

ABSTRACT OF DISSERTATION

ELECTRON-REFLECTOR STRATEGY FOR CdTe THIN-FILM SOLAR CELLS

The CdTe thin-film solar cell has a large absorption coefficient and high theoretical efficiency. Moreover, large-area photovoltaic panels can be economically fabricated. These features potentially make the CdTe thin-film solar cell the leading alternative energy source. However, the record CdTe efficiency (16.5%) is much less than its theoretical maximum efficiency (29%), primarily because the open-circuit voltage (0.845 V) is well below what is expected for its band gap (1.5 eV). The incorporation of an electron reflector is a strategy to improve the open-circuit voltage of solar cells, and thus a strong possibility to improve the efficiency of CdTe thin-film solar cells.

An electron reflector is a conduction-band energy barrier at the back surface of the solar cell, which can reduce the recombination due to the electron flow to the back surface. Different methods to create an electron reflector are explained in the thesis: (1) expanded band gap, either an expanded-band-gap layer or a bulk-band-gap reduction, and (2) alteration to the band bending through a reversed back barrier or a heavily-doped back surface. Investigation shows that the expanded-band-gap layer is the most efficient and practical mechanism for an electron reflector, and the combination of any two mechanisms does not yield additional improvement.

To have the optimal effect from the electron-reflector strategy, reasonable CdTe lifetime (1 ns or above) and full depletion of the CdTe layer are required to ensure high carrier collection. Furthermore, a good-quality reflector interface between the p-type CdTe layer and the electron-reflector layer is essential. Preliminary experimental evidence has shown that CdTe cells with a ZnTe back layer do have a slightly higher open-circuit voltage.

An electron reflector should be particularly beneficial for thin (less than 2 μm) CdTe cells which have a fully-depleted CdTe absorber layer. Thin CdTe cells can also benefit from the optical reflection at the back surface. To investigate the possibility of still higher efficiency, both electron and optical reflection were numerically applied to the CdTe record-cell baseline model. However, there is little improvement for CdTe thicknesses greater than 2 μm. To have the optimal effect from combined electron and optical reflection, cells approximately one micron thick are required. Even without the improvement to the current quality of CdTe, cell efficiency above 19% should be achievable with a 0.2-eV electron reflector. Moreover, efficiency above 20% should be possible if one can also achieve large optical back reflection. At the same time, competitive CdTe cell performance at a thickness as thin as 0.4 um should be possible.

This thesis gives a comprehensive numerical investigation of the electron-reflector strategy for CdTe thin-film solar cells.

Kuo-Jui Hsiao
Department of Physics
Colorado State University
Fort Collins, CO 80523
Spring 2010

Acknowledgements

I would like to thank many people who have helped me while pursuing my degree. This work would not be possible without their help.

First of all, I would like to thank my advisor James Sites, who is always generous and patient with me along the way. Thank you for your guidance, your wise insight, and many great professional opportunities given to me. Working with you is an invaluable experience. Thanks for all the help along the way.

Thanks to my committee members, Martin Gelfand, Robert Leisure, and Walajabad Sampath, for reviewing this work and giving me helpful suggestions. Special thanks to Sampath for giving me the invaluable opportunity to work in his lab.

Thanks to postdocs, Jun Pan and Srinivas Sathiraju, and past and present graduate students, Ana Kanevce, Alan Davies, Galymzhan Koishiyev, Katherine Zaunbrecher, John Raguse, Russell Geisthardt, Pavel Kobyakov, Nathan Schuh, and Nicole Landau, for their help. Jun and Ana, thank you for fruitful discussions. Alan and Galym, thank you for showing me solar-cell characterizations. Katherine and Paul, thank you for proofreading my thesis. Srinivas and Nathan, thank you for letting me work with you, so I could learn cell fabrication.

Thnaks to Tim Gessert and Joel Duenow in National Renewable Energy Labtorary for the finish of cells.

Thanks to my parents, Fu-Feng Hsiao and Min Teng, for their endless encouragement and love from the other side of the earth.

This work was supported in part by Abound Solar through the U.S. Department of Energy's photovoltaic incubator program. Simulations used the software AFORS-HET v2.2, developed in Hahn-Meitner-Institut Berlin with support from the German Bundesministerium für Bildung und Forschung.

Table of Contents

List of Figures

List of Tables

Chapter 1

Introduction

1.1 Why Alternative Energy?

Energy consumption has increased steadily with civilization development. To sustain human development, more electricity consumption is expected in future decades. Our primary solution to this increasing electricity consumption has been to burn more fossil fuels (coal, oil, or natural gas) or build more nuclear plants. However, the green-house gasses produced by burning fossil fuels have been responsible for global warming, and safe disposal of high-level radioactive waste from nuclear plants raises several issues. These impacts are irreversible, and therefore, alternative energy resources are needed.

1.2 Why Solar Energy?

Renewable energy is generated from natural resources such as sunlight, wind, rivers, and so forth, which are naturally replenished. Environmentally-benign renewable energy should provide a good alternative energy resource. Solar energy is one of the most competitive renewable energy resources. In 2008, the average worldwide energy consumption rate was 15 TW [1]. The solar energy received by the earth is about 130,000

TW, which is much more than what we need to power the world. The sun is about half way through its evolution to its next stage, so theoretically, it will shine for the next six billion years [2]. For practical purposes, it is an infinite energy source. Moreover, the sunlight is accessible nearly everywhere. Based on its long life and accessibility, solar energy is a very potential leading renewable energy source.

1.3 Why CdTe for Thin-Film Solar Cells?

Solar cells are devices which can convert solar energy directly to electricity, and this process is often referred to as photovoltaics (PV). Utilization of solar energy is expensive compared with conventional energy resources. To make the price of solar energy competitive with traditional energy sources, low-cost PV systems are required. There are two approaches to this goal: either higher efficiency or lower cost.

The CdTe (Cadmium Telluride) thin-film solar cell is one of the most competitive photovoltaic devices as far as cost and efficiency are concerned. CdTe has a large optical absorption coefficient. Only a small amount of CdTe (2-8 microns thick) is needed for the absorber layer (100 times thinner than typical crystalline-Si solar cells). Moreover, the band gap of CdTe matches the solar spectrum quite well. It is quite close to the band gap which produces the highest theoretical conversion efficiency.

CdTe solar cells can be fabricated with a variety of deposition techniques, because the electronic properties and the structure are generally optimized by the post-deposition treatment. Economic fabrication processes are already utilized in large-scale manufacturing [3,4]. CdTe can also be deposited on low-cost substrates, such as glasses or plastics. Overall, CdTe cells could be the primary technology to low-cost PV systems.

However, the record CdTe efficiency (16.5%) [5] is well below its theoretical maximum value (~29%) [6], because the open-circuit voltage of the record cell, 845 mV [5], is significantly below what is expected for its band gap (E_g ~ 1.5 eV). In 2006, James Sites and Jun Pan of Colorado State University proposed strategies to increase CdTe solar-cell voltage [7]. Of their two proposed strategies, that of the electron reflector is probably more practical for voltage improvement, because it does not require a major improvement in the quality of thin-film CdTe. To see the full potential of the electron-reflector strategy for CdTe solar cells, a comprehensive investigation described in this dissertation was carried out.

Chapter 2

Background

This chapter contains background information that should be helpful for reading this dissertation. It summarizes the physics of CdTe thin-film solar cells, characterization tools, and one-dimensional numerical simulation.

2.1 Semiconductors

Every atom has a set of discrete electron energy levels. As several atoms are brought closer to one another, the original energy levels spread into energy bands. The highest energy band containing electrons is defined as the valence band, and the conduction band is defined as the energy band where electrons can conduct net current by moving through the unoccupied energy states. The gap in energy between the lowest energy of the conduction band E_C and the highest energy of the valence band E_V is the forbidden band, where in the ideal case, no energy states are allowed. Doping impurities and unintentional defects, however, exist in the forbidden band and are responsible for most semiconductor applications. The energy defining the forbidden band is the band gap, $Eg = E_C - E_V$.

The Pauli exclusion principle says that each quantum state can only be occupied by one electron. Therefore, in the ground state, electrons start filling the energy levels from the lowest energy. The energy of the topmost filled level in the ground state is defined as the Fermi energy E_F. At finite temperature, however, the system is no longer in the ground state, and some electrons will fill higher energy states. The probability of the occupation of an allowed energy state at a given energy E is given by the Fermi-Dirac distribution function:

$$F(E) = 1/\{1 + \exp [(E - E_F)/kT]\} \qquad (2.1)$$

where k = Boltzmann constant = 1.38×10^{-23} J/K and T = absolute temperature.

The band structure governs the characteristics of solids. Fig. 2.1 shows the band diagrams of different solids. A solid with either a partially filled conduction band or overlapping conduction and valence bands has a zero band gap. In this solid, electrons subject to a small applied field are free to move. Therefore, this solid is a conductor (see fig. 2.1(a)). In an insulator (see fig. 2.1(b)), the band gap is so large that essentially no electrons can be excited to conduction band to contribute to the current flow. In a semiconductor, the band gap is relatively narrow (see fig. 2.1(c)). At low temperature, a semiconductor material behaves like an insulator. At higher temperature, however, there is a reasonable probability of electron excitation from the valence band to the conduction band, so electrons can contribute to the current in the conduction band. In the valence band, electrons also conduct net current through the unoccupied energy states, which are referred to as holes. Instead of considering the motion of electrons in the valence band, it can be more simply described as the motion of a hole in the opposite direction. Fig. 2.2 shows a schematic explaining this equivalence. Hence, the sum of the motion of electrons

in the conduction band and holes in the valence band contributes to the current flow in a semiconductor.

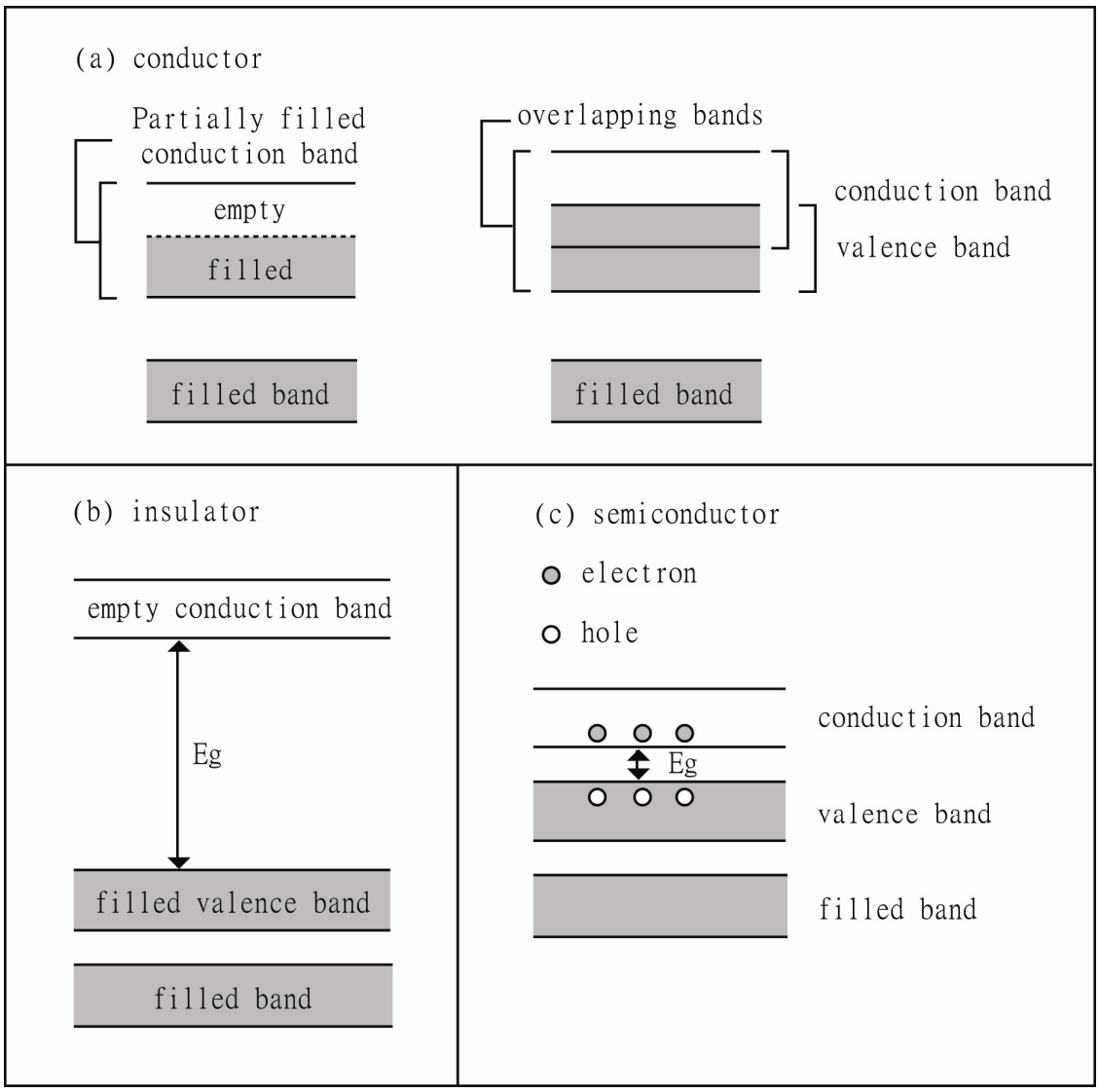

Fig. 2.1 Schematic energy bands of (a) a conductor, (b) an insulator, and (c) a semiconductor.

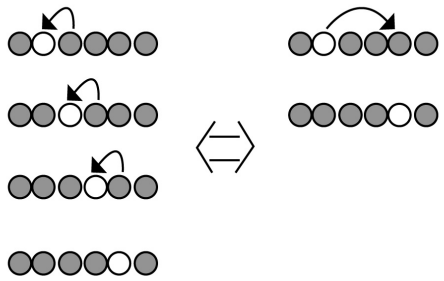

Fig. 2.2 The movement of valence-band electrons can be simply described as the movement of a valence-band hole in the opposite direction.

2.2 Semiconductor Properties

A semiconductor which contains a negligible amount of impurities compared with the thermally generated carriers is an intrinsic semiconductor. In thermal equilibrium, which means the steady state condition at a given temperature without external excitations such as light or electric field, the electron density, or n, in the conduction band is given by integrating the electron density at a given energy n(E) with respect to energy E from E_C to the energy at the top of the conduction band E_{TOP}. The electron density at a given energy is the product of the Fermi-Dirac distribution function and the density of allowed energy states at a given energy N(E). Then n can be derived:

$$n = N_C \exp[- (E_C - E_F)/kT]. \quad (2.2)$$

where N_C is the effective density of states in the conduction band. Similarly, the hole density, or p, in the valence band can be derived:

$$p = N_V \exp[- (E_F - E_V)/kT]. \quad (2.3)$$

where N_V is the effective density of states in the valence band. For intrinsic semiconductors, the electron density in the conduction band is equal to the hole density in

the valence band, that is, $n = p = n_i$, where n_i is the intrinsic carrier density. The intrinsic carrier density can be obtained from equ. (2.2) and (2.3):

$$n_i = (N_C N_V)^{1/2} \exp(- E_g/2kT) \tag{2.4}$$

Semiconductors which are doped with impurities are extrinsic semiconductors. Dopants can create some states in the forbidden band. The dopants which create states with relatively small ionization energy to the conduction band are known as donors. Electrons in the donor states can be ionized to the conduction band at a moderate temperature. A semiconductor doped with donors usually has additional negatively charged carriers and is said to be n-type. Similarly, the dopants which create states with relatively small ionization energy from the top of the valence band are known as acceptors. Electrons can be excited from the valence band to the acceptor states at a moderate temperature, and positively charged holes are left in the valence band. Therefore, a semiconductor doped with acceptors usually has additional positively charged carriers and is said to be p-type. Electrons are the majority carriers and holes are the minority carriers in the n–type semiconductor. On the other hand, holes are the majority carriers and electrons are the minority carriers in the p–type semiconductor. For extrinsic semiconductors, n is generally close to the donor concentration N_D in n-type semiconductors, and p is close to the acceptor concentration N_A in p-type semiconductors. The Fermi energy of extrinsic semiconductors is governed by these formulas:

$$E_C - E_F = kT \ln (N_C/N_D) \tag{2.5}$$

for n-type semiconductors, and

$$E_F - E_V = kT \ln (N_V/N_A) \tag{2.6}$$

for p-type semiconductors. The Fermi energy level of an n-type semiconductor is closer to the conduction band, while that of a p-type semiconductor is closer to the valence band.

The process in which an electron transits from the conduction band to the valence band to annihilate an electron-hole pair is called recombination. There are three different recombination mechanisms: (a) Radiative recombination: It is a reverse process of the absorption. It occurs with emitted light and happens more rapidly in direct-band-gap semiconductors. (b) Auger recombination: In this recombination process, the released energy will excite another electron to a higher energy level instead of emitting light. This excited electron will then relax back to its original state by emitting phonons. Auger recombination is especially probable in the heavily doped material. (c) Recombination through traps: Impurities and defects can form energy levels in the forbidden band. Therefore, electrons can relax from the conduction band to these energy levels and then recombine with holes in the valence band. This process is particularly likely if the energy levels are near the middle of the band gap.

Carrier lifetime is defined as the average time it takes for carriers to recombine, and the carrier diffusion length is the average distance these carriers travel before they recombine.

2.3 Semiconductor Junctions

P-N Junction

When an n-type semiconductor and a p-type semiconductor are joined, a p-n junction device is formed. If the materials in the p-type and the n-type regions are the same, the junction is called homojunction, but when the materials in the p-type and the n-

type regions are different, the junction is called heterojunction. Fig. 2.3 shows the schematic and the band diagram for a p-n junction. Due to the gradient of the carrier density, majority-carrier electrons diffuse from the n-type region to the p-type region, and majority-carrier holes diffuse from the p-type region to the n-type region. This carrier diffusion will produce a diffusion current flow from the p-type region to the n-type region. The charged dopants will create a built-in field in the opposite direction to the diffusion current. This build-in field will produce a drift current.

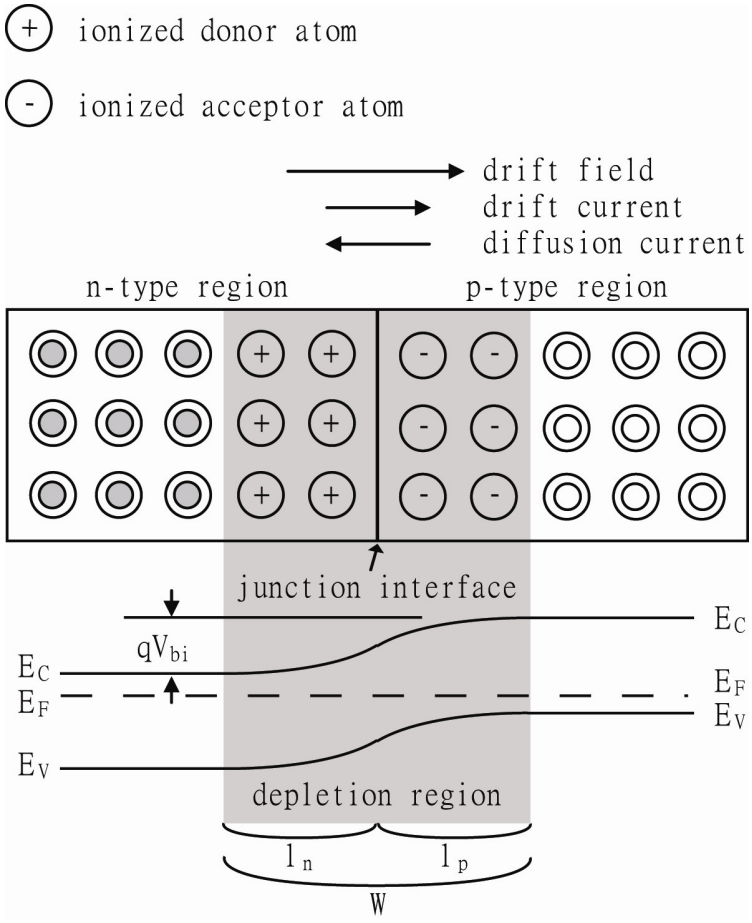

Fig. 2.3 The schematic and the band diagram of a p-n junction.

When the drift current and the diffusion current are equal, equilibrium will be reached, and a depletion region devoid of carriers will be formed at the junction. In equilibrium, the Fermi energy levels in the p-type region and n-type region are aligned to coincide and an electrostatic potential difference exists across the depletion region. This potential difference is called the built-in potential:

$$V_{bi} = kT/q \ln(N_A N_D/n_i^2) \quad (2.7)$$

The width of the depletion region can be calculated by this formula:

$$W = [2\varepsilon/qV_{bi}(1/N_A + 1/N_D)]^{1/2} \quad (2.8)$$

where ε is dielectric constant. The depletion width in the n-type region l_n and that in the p-type region l_p can be calculated by:

$$l_n = WN_D/(N_A + N_D) \text{ and } l_p = WN_A/(N_A + N_D) \quad (2.9)$$

In a forward bias, the positive terminal of the bias source is connected to the p-type material and the negative terminal of the bias source to the n-type material. When a forward bias V_a is applied to a p-n junction. The electrostatic potential across the depletion region will be reduced by V_a, so the depletion width will be modified to be $W = [2\varepsilon/q(V_{bi} - V_a)(1/N_A + 1/N_D)]^{1/2}$, which is smaller than the original value. When N_D is much larger than N_A, $W \approx [2\varepsilon/q(V_{bi} - V_a)(1/N_A)]^{1/2}$ and $l_p \approx W$. The majority of the depletion region is in the region with the lower carrier density. Typically, this is the case for p-type CdTe thin-film solar cells, and the depletion region is a function of the applied voltage and the carrier density of CdTe.

Back Contact of CdTe Solar Cells

When a p-type semiconductor and a metal are joined, the metal acts much like a heavily doped n-type semiconductor. A contact junction with a depletion region $W = [2\varepsilon/qV_{bi}\ (1/N_A)]^{1/2}$ in the adjacent semiconductor is formed due to the band bending resulting from the alignment of the Fermi level. The electron affinity of a semiconductor χ is the energy difference between the vacuum level and E_C of the semiconductor, and the work function of a metal ϕ_m is the energy between the vacuum level and the Fermi level of the metal. When $\chi + Eg \leq \phi_m$, with Eg being the band gap of the p-type semiconductor, a low-resistance ohmic p-type semiconductor/metal contact is formed. When $\chi + Eg > \phi_m$, a Schottky-junction contact is formed. The built-in field in the depletion region of the Schottky junction forms a barrier to the flow of holes from the p-type region to the metal contact. Therefore, this back contact has a negative effect on the cell performance. This back barrier is usually characterized by the back-barrier height $\phi_b = \chi + Eg - \phi_m$.

Fig. 2.4 shows the band diagrams of (a) a p-type semiconductor and a metal with a work function lower than the joint p-type semiconductor, and (b) a Schottky junction formed. CdTe has an electron affinity χ = 4.4 eV and a band gap Eg = 1.5 eV. A metal with a work function greater than or equal to 5.9 eV is therefore required to form an ohmic contact. At room temperature, a back barrier of 0.3 eV or less can effectively form an ohmic contact at the back surface. However, no metal has a work function high enough to make such a contact. Some work functions and back-barrier heights of metals that can be used to make contacts to p-type CdTe are: Cu (ϕ_m = 4.65 eV, ϕ_b = 1.25 eV), Ni (ϕ_m = 5.15 eV, ϕ_b = 0.75 eV), and Ti (ϕ_m = 4.33 eV, ϕ_b = 1.57 eV). One way to

reduce the effect of this back barrier is to heavily dope the back surface of the p-type CdTe layer. The depletion region of the Schottky junction will be thin, and the majority-carrier holes can tunnel through the thinner barrier to form a low-resistance contact.

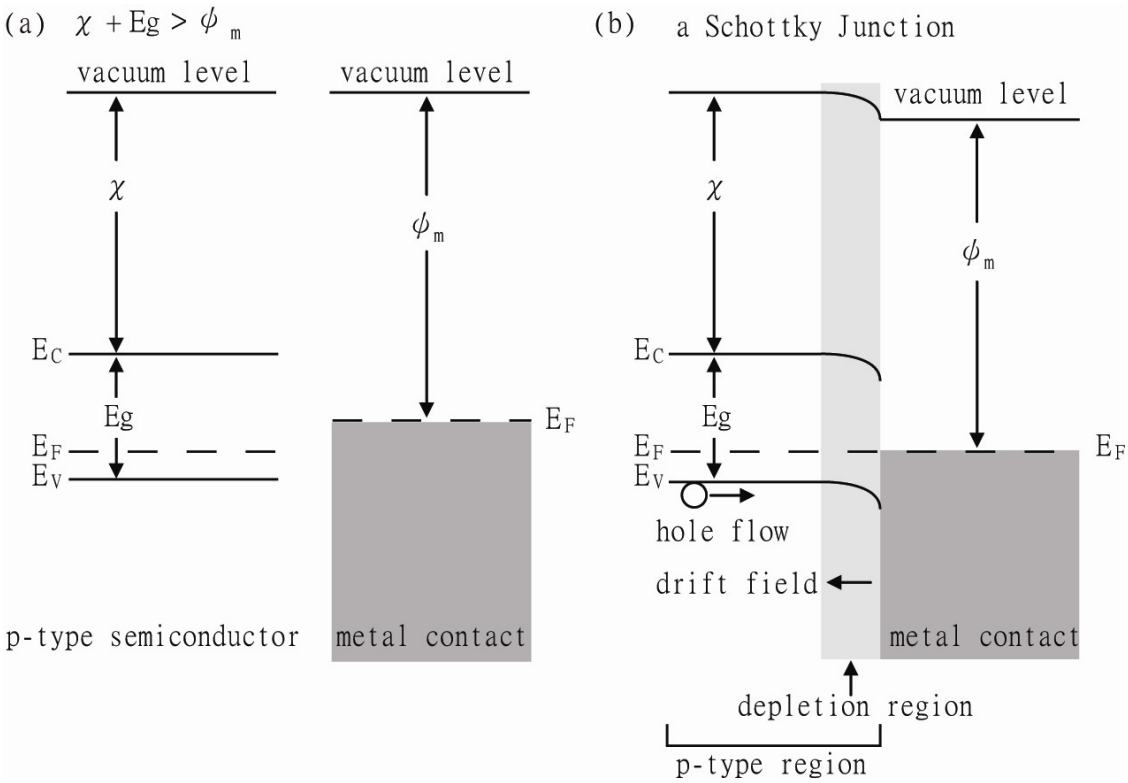

Fig. 2.4 Band diagrams of (a) a p-type semiconductor and a metal contact with a lower work function, and (b) a Schottky junction formed.

2.4 CdTe Thin-Film Solar Cells

The typical configuration of a CdTe thin-film solar cell and its corresponding band diagram are shown in fig. 2.5. In this configuration, glass/transparent-conducting-oxide(TCO)/CdS(n-type)/CdTe(p-type)/metal-contact, the illumination will enter the cell from the glass side, so it is called a superstrate configuration. Glasses with high transmission and good stability are good choices for the superstrates. The TCO is used as

the front contact of the cell. In general, TCO is an n-type semiconductor with a wide band gap (Eg of SnO_2 ~ 3.6 eV), which should minimize optical loss.

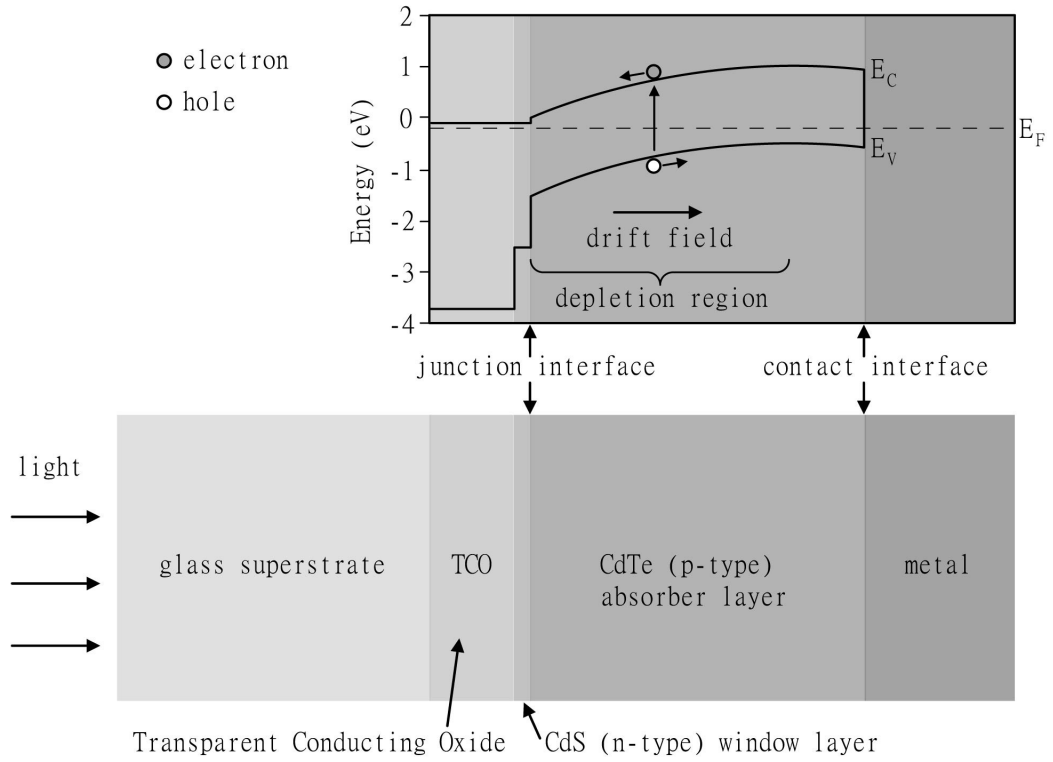

Fig. 2.5 The configuration of a typical CdTe thin-film solar cell and its corresponding band diagram.

A CdTe solar cell is a heterojunction device composed of an n-type CdS layer and a p-type CdTe absorber layer. The CdS has a 2.4-eV (~ 517nm) band gap. Photons with energy larger than its band-gap energy will be absorbed, so a cell with a thick CdS layer allows less blue light to reach the CdTe. With a thin CdS layer, the CdTe and TCO may contact each other in places and form a junction with poorer performance. This will affect the uniformity of the cell. Therefore, a thin CdS layer with a good coverage is preferred. CdTe has a 1.5-eV band gap, which matches the AM 1.5 solar spectrum well. Air mass (AM) at sea level is defined as $1/\cos\theta$ when the sun is at an angle θ from the overhead.

AM 1.5, which corresponds to the sun illumination at 48° from the overhead, is the illumination for standard test conditions.

Typically, the carrier density of the CdTe absorber layer is low ($p = 10^{13}$-2×10^{14} cm^{-3}). With a heavily n-type doped CdS layer ($n = 10^{18}$ cm^{-3}), most of the depletion region is in the CdTe layer. A 2-μm CdTe cell with $p = 10^{13}$ cm^{-3} is fully depleted. Incident light can generate electron-hole pairs in the absorber layer. The built-in field in the depletion region separates electrons from holes to prevent recombination (see fig. 2.5). Then, electrons will flow through the external circuit and recombine with holes in the valence band to complete the cycle. It is preferred to have photons absorbed in the depletion region where light induced carriers can be collected with the assistance of the build-in field. CdTe has high optical absorption in the visible light range. Two microns of CdTe will absorb more than 99% of incident light at 600 nm, so it is a good absorber material for PV applications. A CdTe solar cell usually has a Schottky-barrier contact, but the back CdTe surface can be heavily doped to minimize the negative effect of the Schottky barrier.

2.5 Characterization Techniques

The characterization techniques introduced here include current density versus voltage (J-V) curves and quantum efficiency (QE) curves.

2.5.1 Current Density-Voltage (J-V) Curves

The J-V measurement under standard test conditions (AM 1.5 spectrum and 25 ℃) is the most common tool for solar-cell characterization. The dark J-V curve of an ideal solar cell follows the ideal diode equation:

$$J = J_S(e^{qV/kT} - 1) \tag{2.10}$$

where J is the current density, J_S the saturation current density, and V the applied voltage. When light is applied, the light-induced current flows from the p-type end to the n-type end through the outside circuit. This flow is opposite to the dark current, so the light J-V curve will follow the ideal diode equation shifted by the amount of light-induced current density J_L:

$$J = J_S(e^{qV/kT} - 1) - J_L \tag{2.11}$$

Under realistic conditions, additional parameters need to be considered. For a non-ideal diode, the diode equation will be:

$$J = J_S(e^{q(V - JR)/AkT} - 1) - J_L + G(V - JR) \tag{2.12}$$

where R is the series resistance, G the shunt conductivity, and A is the ideality factor. A = 1 means that ideal diffusion current dominates, whereas A = 2 means that the recombination current dominates. When both currents are comparable, $1 \leq A \leq 2$.

A typical light J-V curve (under standard test conditions) is shown in fig. 2.6. From the light J-V curve, one can extract the open-circuit voltage (V_{oc}), short-circuit current (J_{sc}), fill factor (FF), and efficiency (eff). V_{oc} is the applied forward bias at which no current goes through the solar cell. J_{sc} is the measured induced current density when there is no external bias applied to the solar cell. Power density P is the product of voltage and current density. A P-V curve is shown in fig. 2.6. Its maximum determines

the cell's efficiency. Corresponding maximum power current density and voltage are J_{mp} and V_{mp}. FF is defined as:

$$FF = P_{mp}/(V_{oc}J_{sc}) = (V_{mp}J_{mp})/(V_{oc}J_{sc}). \quad (2.13)$$

FF shows how "square" the J-V curve is. FF = 100% would mean that J-V curve is rectangular. Efficiency is defined as the ratio of the maximum output power to the input power = $(V_{oc}J_{sc}FF)/(100\ mW/cm^2)$, where 100 mW/cm^2 is the power density of the AM 1.5 spectrum.

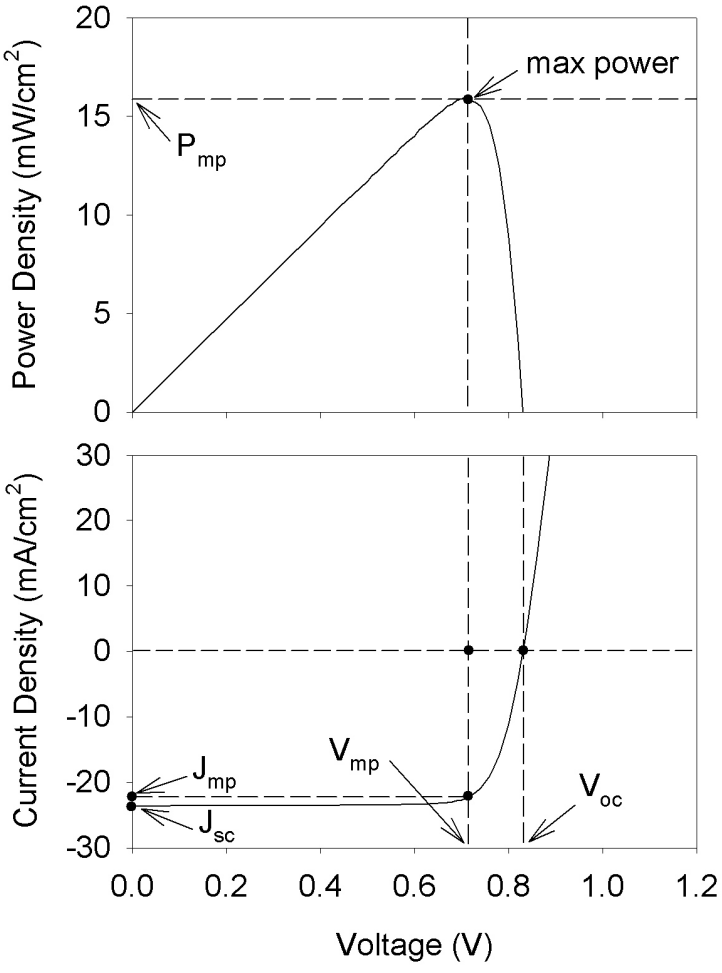

Fig. 2.6 Calculated P-V curve (top) and a calculated J-V curve (bottom) for a typical solar cell.

2.5.2 Quantum Efficiency (QE) Curves

Quantum efficiency is defined as the ratio of electron-hole pairs collected to incident photons at a specified wavelength. Fig. 2.7 shows a calculated QE curve of a CdTe thin-film solar cell with the indication of different losses. QE = 100% means that one incident photon can generate one electron-hole pair. However, the reflection of the superstrate, the absorption of the superstrate, the TCO layer, and the CdS window layer, as well as the incomplete absorption of photons can contribute to the losses.

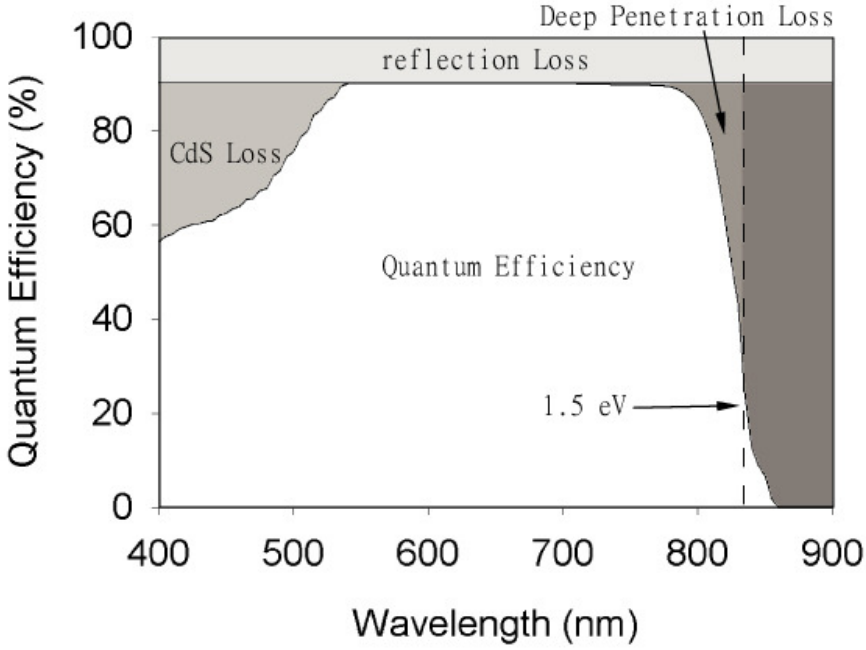

Fig. 2.7 A calculated quantum efficiency curve.

2.6 One-Dimensional Numerical Simulation

One-dimensional numerical simulation of CdTe thin-film solar cells is the investigative approach used in this dissertation. It is a powerful tool to build a reasonable

physical model to test the viability of physical interpretation, and numerical simulations can help predict changes in performance resulting from the modified physical parameters. Moreover, difficult experimental measurements can sometimes be by-passed with simulations.

The operation of semiconductor devices can be described by a set of basic equations. These equations are coupled partial differential equations, for which it is often not possible to find general analytical solutions. These equations can be transformed into a set of nonlinear algebraic equations, which can be solved numerically with a computer. AFORS-HET, (Automat FOR Simulation of HETero-structures), version 2.2 [8] is the software package used in this work to numerically solve the one-dimensional semiconductor equations under steady-state conditions. The basic equations used are:

The Poisson's equation is given by:

$$-\frac{d^2\phi}{dx^2} = \frac{q}{\varepsilon}(p + N_D - n - N_A + \sum_{defects}\rho_t) \tag{2.14}$$

where ϕ is the electron potential. ρ_t is the charge stored in defects, which can be acceptor-like or donor-like. ρ_t is referred to as p_t when the defects are acceptor-like and n_t when the defects are donor-like.

The Continuity equations under steady state conditions are given by:

$$\frac{1}{q}\frac{dJ_p}{dx} = G_p - R_p \tag{2.15}$$

$$-\frac{1}{q}\frac{dJ_n}{dx} = G_n - R_n \tag{2.16}$$

where $G_{p/n}$ is the generation rate for holes/electrons, which in the case of solar cells results from the optical excitation from the solar spectrum. It is important, however, to also know the absorption coefficient of the material at each wavelength to determine $G_{p/n}$ as a function of x. $R_{p/n}$ is the recombination rate for holes/electrons, which was discussed in section 2.2. The hole current J_p and electron current J_n are given by the sum of drift and diffusion currents:

$$J_p = q\mu_p pE - qD_p \frac{dp}{dx} \tag{2.17}$$

$$J_n = q\mu_n nE + qD_n \frac{dn}{dx} \tag{2.18}$$

where $\mu_{p/n}$ is the mobility for holes/electrons, and $D_{p/n}$ is the diffusivity for holes/electrons. Mobility and diffusivity are in general related by Einstein relation:

$$D_{p/n} = \frac{kT}{q}\mu_{p/n} \tag{2.19}$$

On the right hand side of equations (2.17) and (2.18), the first term is the drift current, and the second term is the diffusion current. The continuity equations account for variations in the hole density and electron density of the system.

The electric potential ϕ, the electron density n, and the hole density p are independent variables in this system. All other variables in the equations and boundary conditions are expressed in a way that they only depend on these independent variables. To numerically solve the semiconductor equations, AFORS-HET allows one to build a discrete set of grid points for the device model, and the semiconductor equations are

solved at each of these. At the grid points on the two ends of the device, the electric potential, hole current, and electron current need to satisfy specified boundary conditions. The starting solution of each grid point in the device can be the last calculated solution, the analytical approximation provided by the program, or a specified starting solution. The independent variables, including ϕ, p, and n, at each grid point can be determined by solving the basic equations for each interval with the proper boundary conditions. Once we determine ϕ, p, and n throughout the cell with specific boundary conditions, illumination, and temperature, we can solve for the band diagrams, J-V curves, and other characteristics.

To investigate the electron-reflection strategy with the one-dimensional numerical simulation, a four-layer device model CdS/bulk-CdTe/electron-reflector/ metal-back-contact for CdTe thin-film solar cells is used. Fig. 2.8 shows the band diagram of the four-layer model.

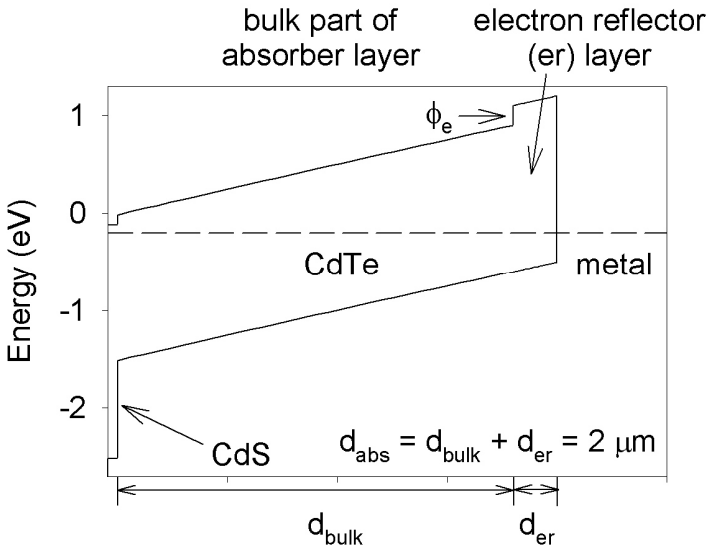

Fig. 2.8 Band diagram of the simulation model

A baseline parameter setting [9] with minor adjustment was assigned to this model. Table 2.1 shows the parameters of the baseline cell. The values used have been either determined by independent measurements or are reasonable estimates. External reflection of the superstrate was assumed to be 10%. A 0.3-eV back barrier height corresponds to a flat band at the back surface with $p \sim 10^{13}$ cm^{-3}. The surface recombination velocity S is given by:

$$S = N_s \sigma v_t \tag{2.20}$$

where N_s is the defect density at the surface and v_t thermal velocity. With $N_s = 10^9$ cm^{-2},

Contact Interface			
	Front		**Back**
Barrier Height (eV)	0.1 (E_C-E_F)		0.3 (E_F-E_V)
S_e (cm/s)	10^7		10^7
S_h (cm/s)	10^7		10^7
Semiconductor Layer			
	SnO_2 (TCO)	**CdS (n-type)**	**CdTe (p-type)**
d (nm)	500	45	1800
$\varepsilon/\varepsilon_0$	9	10	9.4
E_g (eV)	3.6	2.4	1.5
N_C (cm^{-3})	2.22×10^{18}	2.22×10^{18}	7.8×10^{17}
N_V (cm^{-3})	1.8×10^{19}	1.8×10^{19}	1.8×10^{19}
μ_e (cm^2/Vs)	100	100	320
μ_h (cm^2/Vs)	25	25	40
N_A, N_D (cm^{-3})	$N_D = 10^{17}$	$N_D = 1.1\times10^{18}$	$N_A = 10^{13}$
χ (eV)	4.5	4.5	4.4
Gaussian (Midgap) Defect States			
	SnO_2 (TCO)	**CdS (n-type)**	**CdTe (p-type)**
N_{DG}, N_{AG} (cm^{-3})	D: 10^{15}	A: 10^{18}	D: 9×10^{10}
W_G (eV)	0.1	0.1	0.1
σ_e (cm^2)	10^{-12}	10^{-17}	10^{-9}
σ_h (cm^2)	10^{-15}	10^{-14}	10^{-12}

Table 2.1 Parameters of the baseline cell. Index e/h represents electrons/holes, S surface recombination velocity, d thickness, $\varepsilon_0 = 8.85\times10^{-12}$ F/m electric constant, $N_{DG/AG}$ the donor-like/acceptor-like defect density, W_G the energy width of the Gaussian distribution for the defect states, τ carrier lifetime, and σ capture cross section.

$\sigma = 10^{-9}$ cm^2, and $v_t = 10^7$ cm/s, S equals 10^7 cm/s, which is the order of the thermal velocity at room temperature. Physically, this means that nearly all electrons will recombine at the back surface at room temperature. Lifetime τ is given by:

$$\tau = 1/(\sigma v_t N_{AG/DG}) \tag{2.21}$$

The lifetime for the baseline setting is 1 ns, which is currently achievable [10]. Donors and acceptors are assumed to be completely ionized, so $p = N_A$ and $n = N_D$. The electron-reflector layer has a 200-nm layer thickness and the other properties the same as CdTe layer for the baseline setting. In this model, the absorber layer, including the bulk CdTe layer and the electron-reflector layer, is fixed at 2 μm. With the baseline $p = 10^{13}$ cm^{-3}, the cell is fully depleted, which is important, because it means there will be an electric field throughout the CdTe. Full depletion and reasonable lifetime (1 ns or above) are optimal conditions, which are discussed in section 3.3. An electron reflector can be created by changing the band gap or the carrier density of the electron-reflector layer. The detail will be explained in section 3.

All band structures, J-V curves, and QE curves in this dissertation are calculated results based on the approach mentioned above, except for experimental data from references in chapter five and the experimental results in chapter six.

Based on this simulation model, a reasonable baseline cell (J_{sc} = 24 mA/cm^2, V_{oc} = 830 mV, FF = 81%, R_s = 1 Ω·cm^2, G = 0.2 mS/cm^2, and eff = 16%) is utilized. Fig. 2.9 shows the calculated J-V curve of the baseline cell. This baseline cell has a 1-ns carrier lifetime, a 10^{13}-cm^{-3} hole density, and a 2-μm absorber layer. The electron-reflector barrier height is 0 eV (no electron reflector) for the baseline cell.

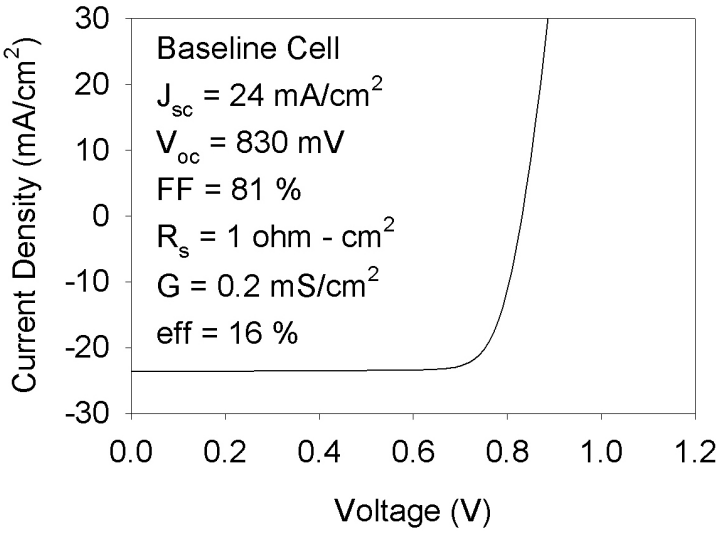

Fig. 2.9 The calculated J-V curve of the baseline cell.

Chapter 3

Electron Reflector for CdTe Solar Cells

In this chapter, the formation and the effect of the electron reflector for CdTe thin-film solar cells are investigated, and different mechanisms to create an electron reflector are explained. Then, the cell conditions needed for the optimal effect of the electron-reflector strategy will be explored. Finally, related issues, such as interfacial recombination and valence-band offset at the interface between the bulk CdTe layer and the electron-reflector layer, will be discussed. "ER" will be used to abbreviate electron reflector through the remainder of the thesis.

3.1 Introduction

A back-surface field (BSF) has been used to improve the performance of Si-based solar cells for many years [11-15]. For many solar cells, there are many allowed states within the forbidden gap at the back surface, and recombination can occur efficiently through these states. When the minority-carrier diffusion length is longer than the cell thickness, back-surface recombination may become the primary limitation on cell performance. In a typical BSF Si-based solar cell, the back surface is heavily doped by

aluminum, and a conduction-band barrier to the forward electron flow is created. The built-in field at the back surface can drive carriers away from the back surface to result in an effective back-surface recombination velocity which is much lower than that in the absence of the BSF, especially at forward bias. Therefore, the open-circuit voltage can potentially be improved. The BSF also increases the collection probability for carriers generated near the back contact and hence boosts the long-wavelength photon collection. Overall, both open-circuit voltage and short-circuit current can be increased by reduced back-surface recombination. Such improvements have been obtained experimentally [16, 17]. If the cell thickness is reduced, the bulk recombination which occurs is proportionally reduced, and if the cell thickness is reduced to be comparable to the diffusion length, the back-surface recombination dominates and lowers the open-circuit voltage. Under this condition, the BSF is particularly useful to reduce the back-surface recombination, and allow higher open-circuit voltage. Hence, the BSF allows thinner absorber layer with acceptable performance [16].

This BSF strategy is referred to as an electron reflector in this work, simply to be more physically descriptive. The incorporation of an electron reflector to improve the open-circuit voltage of CdTe thin-film solar cells was investigated numerically in reference [18]. Fig. 3.1 shows the band diagrams of a baseline CdTe solar cell at (a) zero bias and (b) V_{bias} = V. Fig 3.1 (c) shows the band diagram of a CdTe cell with an electron-reflector layer at V_{bias} = V. Carriers can be collected efficiently with the assistance of the built-in field in the depletion region where the bands are not flat. In a fully depleted cell as shown in fig 3.1 (a), the built-in field can drive electrons in the conduction band across the cell away from the back surface. At forward bias, the field is

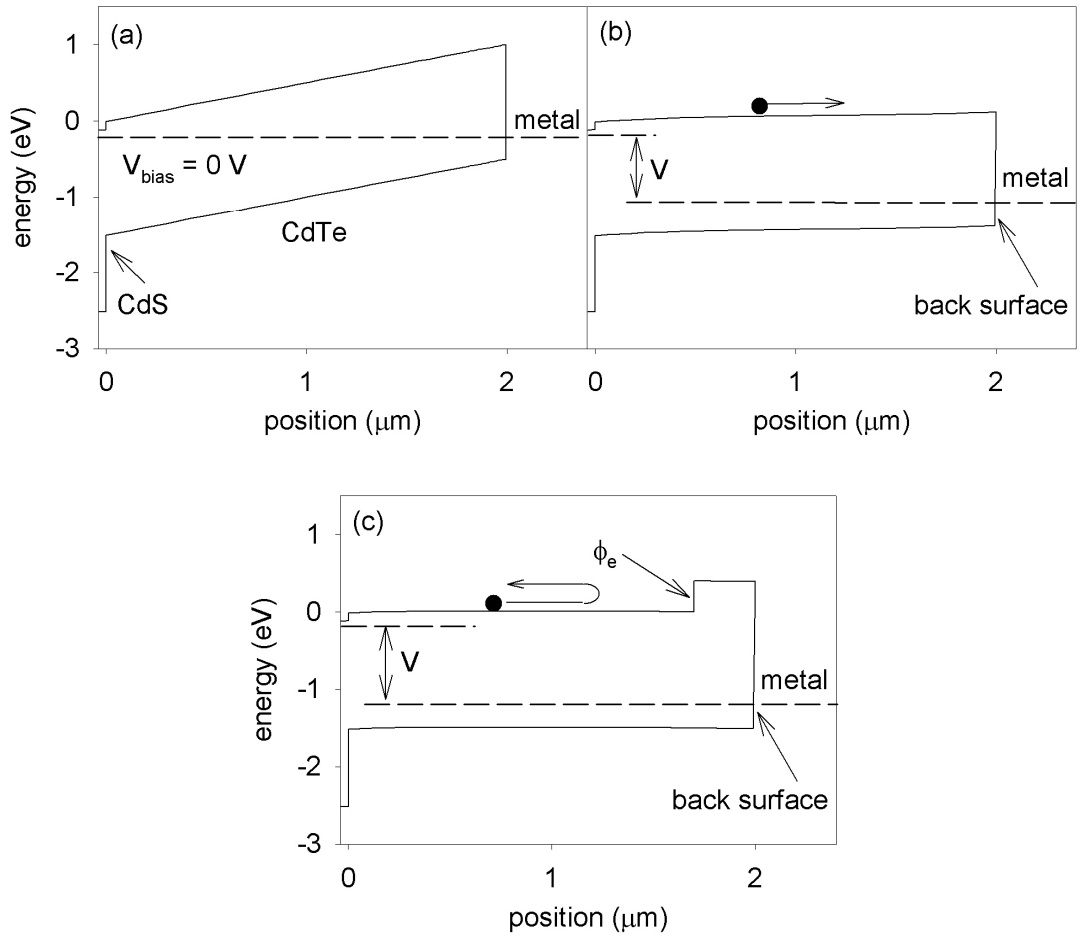

Fig. 3.1 Band diagrams of a baseline CdTe solar cell at (a) zero bias and (b) V_{bias} = V. (c) The band diagram of a CdTe cell with an electron-reflector layer at the back surface.

reduced, and it can be reduced too much to drive carriers (see fig 3.1 (b)). Then more minority-carrier electrons can flow to the back surface. If there is a conduction-band barrier at the back surface, it can keep electrons away from the back surface (see fig. 3.1 (c)). Therefore, the recombination resulting from the forward electron flow to the back surface will be reduced, especially at forward bias. This conduction-band barrier is defined as an electron reflector. The primary parameter is the electron-reflector barrier height ϕ_e.

Typically, CdTe cells have short diffusion length (few micrometers at a typical 1-ns lifetime). The diffusion length L_e can be calculated by the equation:

$$L_e = (D_e \tau_e)^{1/2} \quad (3.1)$$

The built-in electric field in the depletion region, often referred to as the drift field, can be used to increase the carrier collection, and thus to reduce the bulk recombination. It should be particularly beneficial for CdTe thicknesses below 2 μm when the CdTe is fully depleted at a typical carrier density.

Back-surface recombination can significantly degrade the open-circuit voltage of CdTe cells. The common parameter to quantify it is the back-surface recombination velocity for majority-carrier holes S_b. Fig. 3.2 (a) shows the calculated J-V curves for a fully depleted CdTe cell with no electron reflector. Parameters for fig. 3.2 are d_{abs} = 2 μm, $p = 10^{13}$ cm^{-3} and ϕ_b = 0.3 eV. These curves illustrate the voltage difference with a series of values for S_b =10^7, 10^4, and 10^1 cm/s. On the other hand, fig. 3.2 (b) shows the calculated J-V curves for fully depleted cells with $S_b = 10^7$ cm/s and different electron-reflector barrier heights (0, 0.2, and 0.3 eV). These curves show the effect of an electron reflector on the open-circuit voltage. There is some equivalence between lower S_b and larger ϕ_e. Both increase V_{oc} by reduced the back-surface recombination, and one can say that the electron reflector reduces the effective value of S_b. Note that several orders of magnitude in S_b are needed to match the electron-reflector improvement. Therefore, the electron reflector is potentially an efficient way to improve V_{oc} by reducing the back-surface recombination. The calculated values of J_{sc} and FF change only slightly with S_b or ϕ_e. Fig. 3.3 summarizes the effect of varied S_b (10^1-10^7 cm/s) and ϕ_e (0, 0.2, and 0.3 eV) on V_{oc} assuming a 1-ns lifetime (fig. 3.3 (a)) and a 10-ns lifetime (fig. 3.3 (b)). When

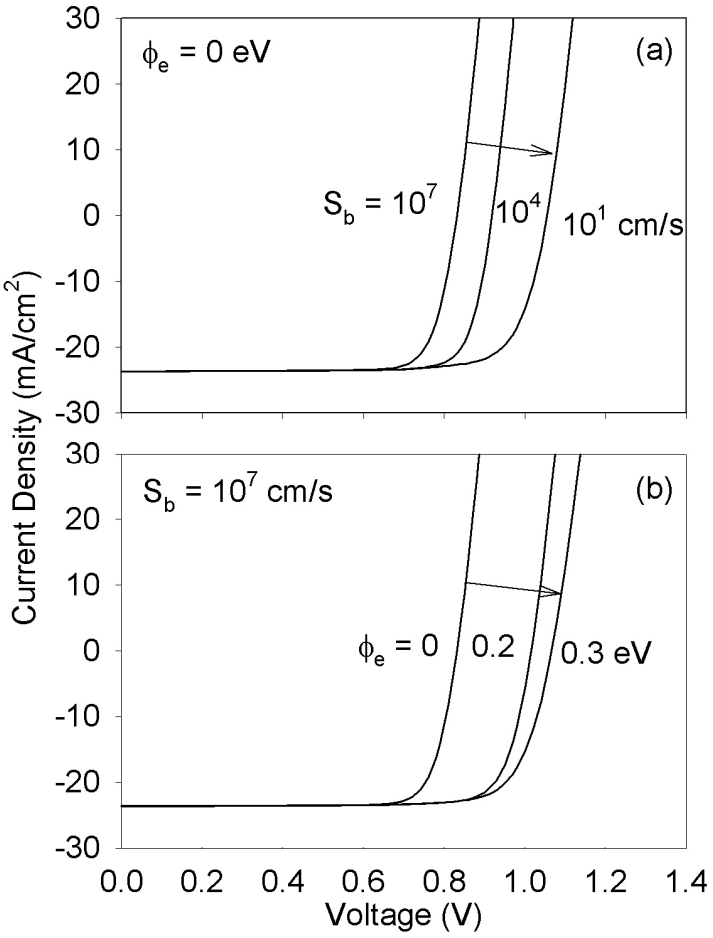

Fig. 3.2 (a) Calculated J-V curves of cells with varied S_b and no electron reflector (ϕ_e = 0 eV). (b) Calculated J-V curves of cells with $S_b = 10^7$ cm/s and varied ϕ_e.

S_b is above 10^6 cm/s, the V_{oc} improvement is initially very nearly equal to ϕ_e/q, but saturates above a 200 mV increase for a 1-ns lifetime, and above 300 mV for higher lifetimes. With smaller S_b, the base V_{oc} is larger, and the electron-reflector improvement is less. With any value of S_b, larger V_{oc} should be achieved with a larger lifetime of the absorber layer, especially when the back-surface recombination is reduced by a lower S_b or higher ϕ_e. Based on this simulation, V_{oc} greater than 1 V should be achievable with a 0.2-eV electron reflector and a currently achievable lifetime (1 ns) [10]. In the next section, four mechanisms to create an electron reflector will be explained.

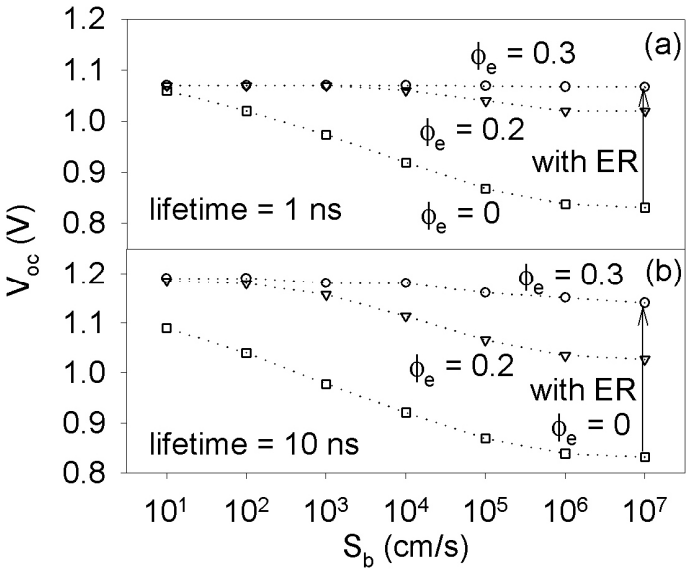

Fig. 3.3 The effect of S_b and ϕ_e variations on V_{oc} with (a) 1-ns lifetime and (b) 10-ns lifetime.

3.2 Mechanisms to Create an Electron Reflector

We can create an electron reflector either by having an expanded-band-gap layer at the back surface or by band bending. Fig. 3.4 shows the various schematics of mechanisms to create an electron reflector. The schematic of the expanded-band-gap layer is shown in fig. 3.4 (a). To have an expanded-band-gap layer, one can either increase the band gap of the electron-reflector layer (Eg_{ER}) or reduce the band gap of the bulk part of the absorber layer (Eg_{bulk}). There are two mechanisms that can create an electron reflector by band

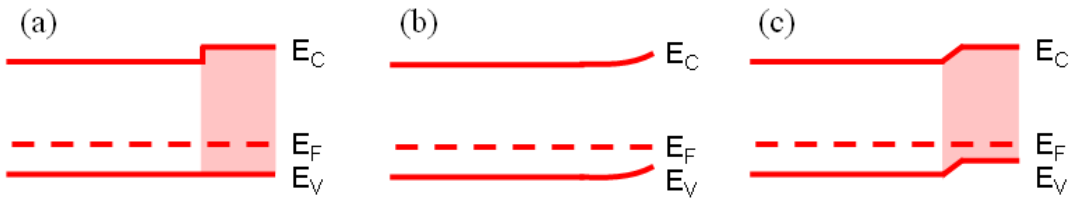

Fig. 3.4 Schematics of mechanisms to create an electron reflector: (a) expanded-band-gap layer, (b) reversed back barrier, and (c) heavily-doped back surface.

bending. They are a back-contact barrier opposite to the normal direction (fig. 3.4 (b)) and a heavily-doped back surface (fig. 3.4 (c)). Due to the alignment of Fermi level, each of these two possibilities can create a conduction-band barrier at the back surface. These four mechanisms of the electron-reflector strategy for CdTe solar cells will be investigated below.

3.2.1 Expanded Band Gap

This kind of electron reflector can be abrupt and the barrier height remains constant with external bias. The material of the electron-reflector layer needs to have a higher band gap than that of the bulk part of the absorber layer with the increase primarily happening in the conduction band. As a result, the barrier height ϕ_e is approximately the difference between band gaps as shown in fig. 3.1 (c). Two mechanisms to create this type of electron reflector are expanded-band-gap layer, and bulk-band-gap reduction with a small CdTe layer at the back.

3.2.1.1 Expanded-Band-Gap Layer

When an expanded-band-gap layer with an expanded band gap and a negligible valence-band offset is added to the CdTe absorber layer, an electron reflector is created. In this case, the Eg_{bulk} is kept at 1.5 eV, and the reflector layer has a higher band gap than 1.5 eV. The possible materials for an expanded-band-gap layer are CdZnTe, CdMnTe, and CdMgTe. The electron-reflector barrier height will be ϕ_e. The calculated effect on voltage was shown in fig. 3.3. The details depend on the physical parameters of the cell, including those of the added layer.

Electron Reflector vs. Lifetime

In this simulation, a fully-depleted CdTe cell with the baseline parameters mentioned above is augmented by a 200-nm electron-reflector layer. Fig 3.5 shows the calculated effect of lifetime on V_{oc} with varied ϕ_e (0, 0.1, 0.2, and 0.3 eV). V_{oc} initially increases with ϕ_e at a slope near one, but increase saturates near ϕ_e = 0.2 eV with a 1-ns lifetime, and above 0.3 eV for higher lifetimes. A 0.2-eV electron reflector with a currently achievable lifetime (1 ns) should enable a V_{oc} above 1 V without saturating the V_{oc} improvement. If higher lifetimes can be achieved, the V_{oc} could increase even more.

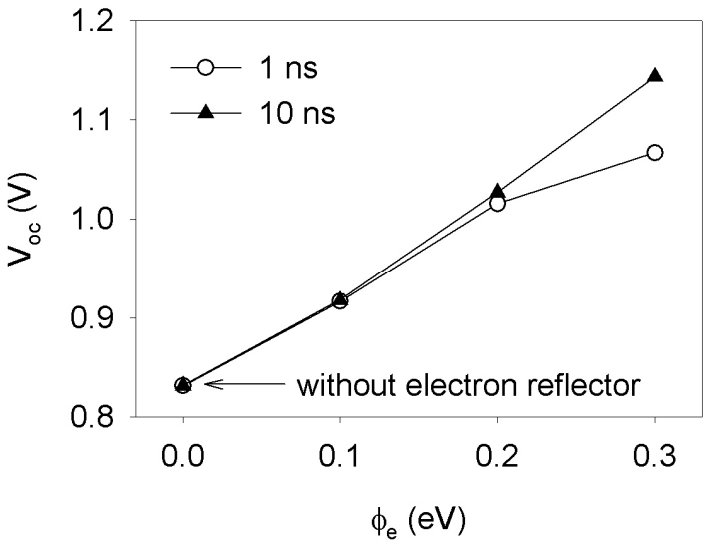

Fig. 3.5 Calculated effect of lifetime on V_{oc} with varied electron-reflector barrier heights.

Electron Reflector vs. Carrier Density

In this simulation, the carrier density of the absorber layer is varied from 10^{13} to 3×10^{15} cm^{-3}. Fig. 3.6 (a) shows the conduction bands of cells over a range of carrier densities, and fig. 3.6 (b) shows calculated corresponding J-V curves for each carrier

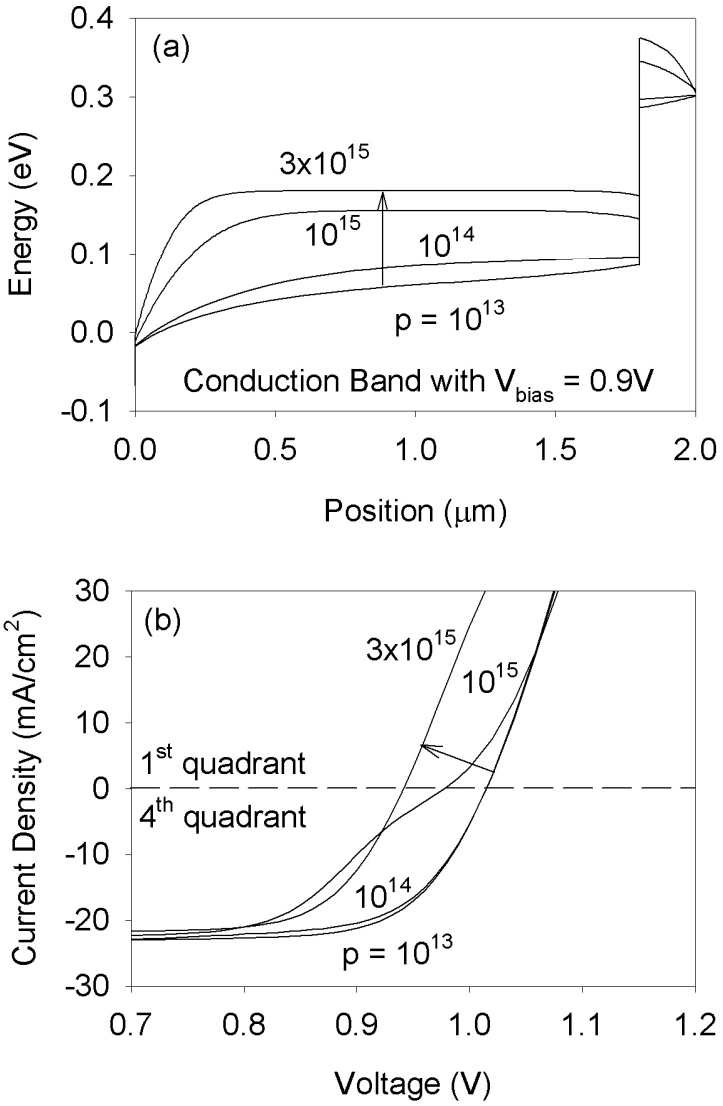

Fig. 3.6 (a) Conduction bands of cells with varied carrier densities with $V_{bias} = V_{oc}$. (b) Calculated J-V curves with varied carrier densities.

density. At higher carrier densities, the cell is not always fully depleted, and the conduction band in the absence of an internal field remains flat (see fig. 3.6 (a)). The corresponding J-V curves (see fig. 3.6 (b)) show that the fully depleted cell ($p = 10^{13}$ cm^{-3}) and the nearly fully depleted cell ($p = 10^{14}$ cm^{-3}) have similar J-V curves with good performance, but the electron-reflector enhancement is significantly diminished in non-fully depleted cells ($p > 10^{14}$ cm^{-3}). That is because the carrier collection is enhanced by

the electric field, which is only fully effective when it extends throughout the CdTe. The curve with p = 10^{15} cm^{-3} shows a transition between the two curves where the voltage dependant depletion width no longer extends throughout the CdTe. We refer to the transition as a kink, because the second derivative of the J-V curve is negative. The kink can exist in the first (p = 3×10^{15} cm^{-3}) or fourth quadrant (p = 10^{15} cm^{-3}). A first-quadrant kink limits the V_{oc} improvement, and a forth-quadrant kink decreases the FF. The existence of kink in either case compromises the maximum output power.

Electron Reflector vs. Layer Thickness

In this simulation, the thickness of the electron-reflector layer d_{ER} was varied from 50 to 500 nm. Fig. 3.7 shows the calculated V_{oc} of cells with different d_{ER}. The result illustrates that the thickness of the electron-reflector layer has little effect with d_{ER} above 200 nm, and intuitively, unless the electrons tunnel, one expects it is only the barrier height and not the thickness that matters.

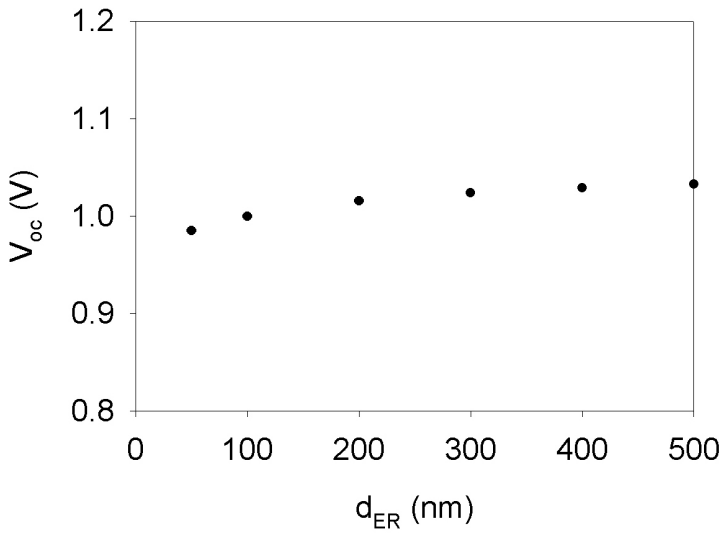

Fig. 3.7 Calculated J-V curves for three different thicknesses of the electron-reflector layer.

3.2.1.2 Bulk-Band-Gap Reduction

In this section, the band gap of the reflector layer (Eg_{ER}) is kept at 1.5 eV, and Eg_{bulk} is reduced to create a conduction-band offset. One would expect a qualitatively similar result. The possible material for bulk-band-gap reduction is CdHgTe. However, the reduction of the band gap shifts the optical absorption spectrum. A reasonable assumption, which is approximately correct for many semiconductor alloys, is that the spectrum shifts in energy by the same amount as the band-gap change. Fig. 3.8 shows the presumed shifts in absorption spectrum for CdTe and closely-related alloys. The absorption coefficient α is defined as:

$$\alpha = 4\pi k/\lambda \tag{3.2}$$

where k is the extinction coefficient and λ is the wavelength.

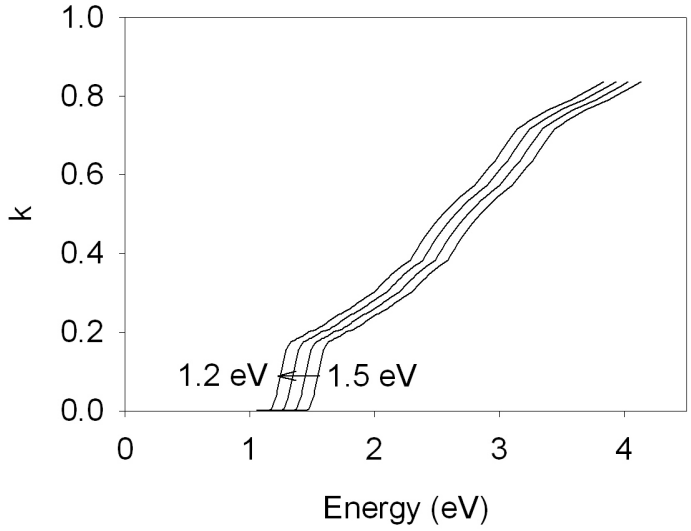

Fig. 3.8 The artificial optical absorption spectra for varied band gaps.

Fig. 3.9 (a) shows two band diagrams with Eg_{bulk} = 1.3 eV and 1.5 eV. In both cases, the back layer is set to 1.5 eV. The calculated corresponding J-V curves shown in

fig. 3.9 (b) illustrate that the reduction of band gap increases the J_{sc}. The bulk layer can absorb photons with energy above Eg_{bulk}. With the bulk-band-gap reduction, more photons can be absorbed.

Fig. 3.10 summarizes the effect of bulk-band-gap reduction on solar-cell parameters. Open triangles represent cells with band-gap reduction and no electron reflector. Solid circles represent cells with band-gap reduction and electron reflector

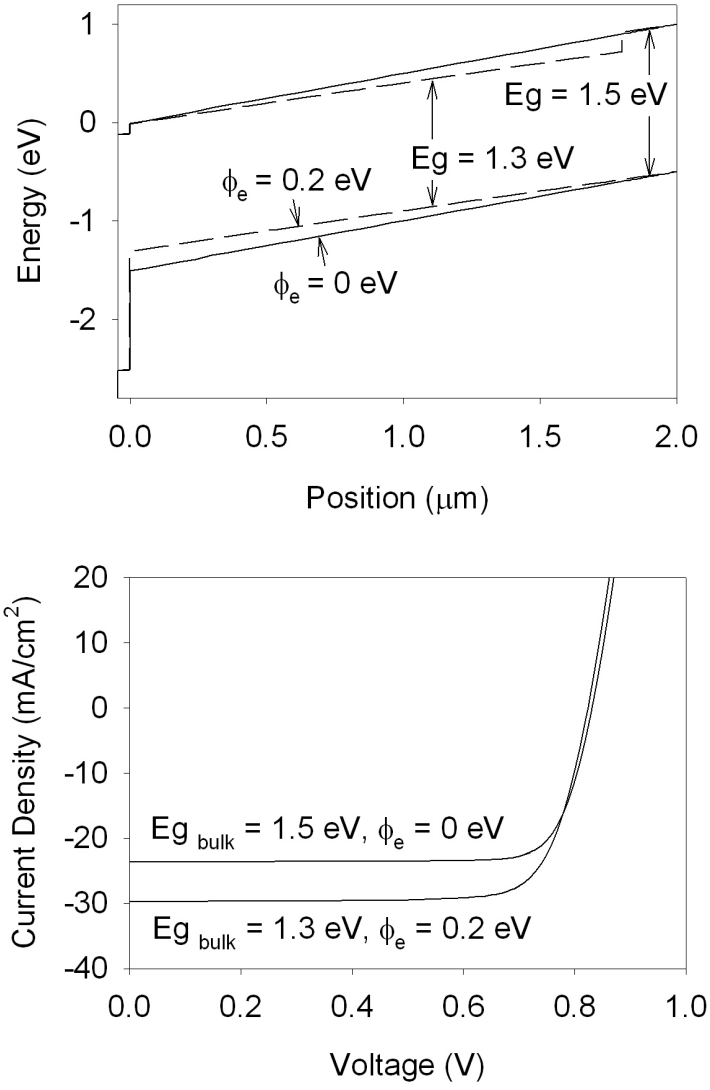

Fig. 3.9 (a) The band diagram of the band-gap-reduction strategy. It is a 0.2-eV band-gap reduction (Eg_{ER} = 1.5 eV, Eg_{bulk} = 1.3 eV). (b) The calculated corresponding J-V curves.

(Eg_{ER} = 1.5 eV and $\phi_e = Eg_{ER} - Eg_{bulk}$). With a 1.5-eV reflector layer, the V_{oc} is maintained near 800 mV, but the lower band gap of the bulk layer allows a higher J_{sc}. A 0.2-eV bulk-band-gap reduction is predicted to have an increase of 6.5 mA/cm^2 in current density and 3% in efficiency, which is essentially equivalent to the expanded band gap.

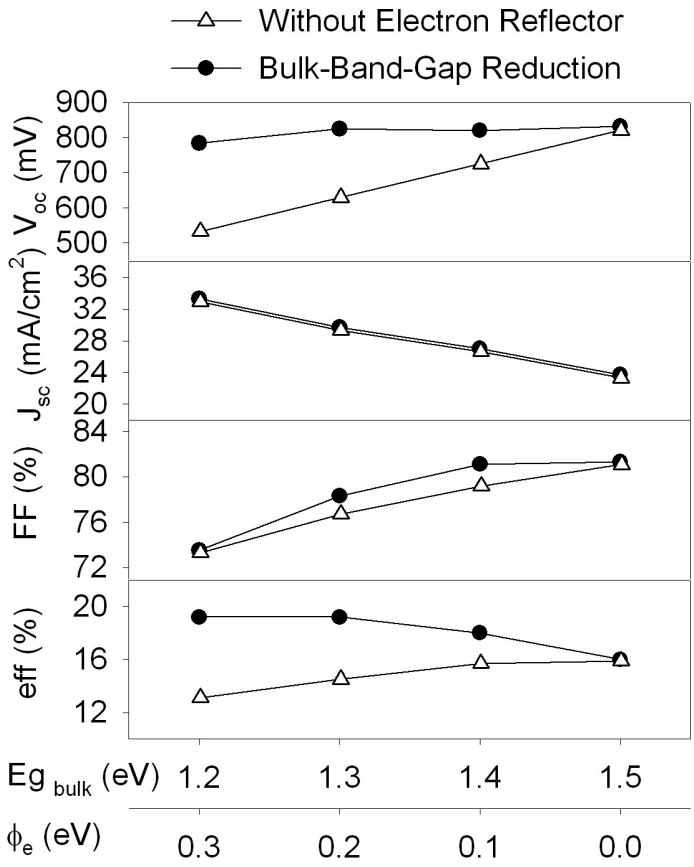

Fig. 3.10 The calculated effect of band-gap reduction on parameters. $Eg_{ER} = Eg_{bulk} + \phi_e$.

△ △ △ △ △ △ △ △ △ △ △ △ △ △ △

The expanded-band-gap strategy can increase either V_{oc} with an expanded-band-gap layer or J_{sc} with the bulk-band-gap reduction. Another method to form an electron reflector is with band bending.

3.2.2 Band Bending

In this section, the conduction-band barrier is created by upward curvature of the bands with respect to the Fermi level near the back surface due to a reversed back barrier or a heavily-doped back surface. This type of electron reflector produces a gradual conduction-band barrier and the barrier height may vary with the external bias. Here, we will focus on the effect of conduction-band offset due to the two mechanisms.

3.2.2.1 Reversed Back Barrier

A back-contact barrier for the majority-carrier holes usually has a negative effect on the cell performance. A back barrier resulting from a metal contact with a very high work function, however, could in principle create a barrier to the electron flow towards the back contact, and therefore be beneficial to the cell performance. Fig. 3.11 shows band diagrams of cells with (a) a back barrier for majority-carrier holes and (b) a back barrier for minority-carrier electrons.

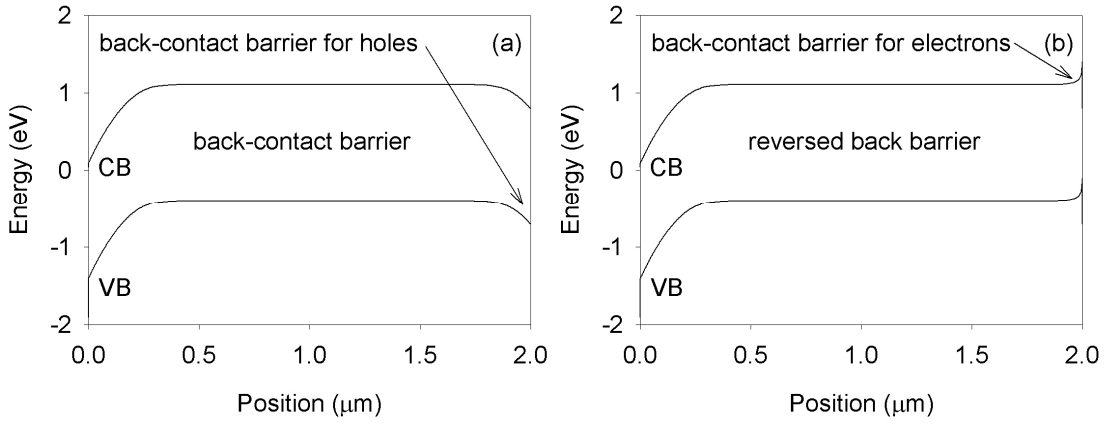

Fig. 3.11 Band diagrams of cells with a back barrier for majority-carrier holes (a) and with a back barrier for minority-carrier electrons (b).

In this simulation, which will be referred to as a reversed back barrier, a cell with a 1-ns lifetime and no expanded-band-gap electron reflector is considered. Fig. 3.12 shows the conduction bands of a lightly-doped fully-depleted cell ($p = 10^{13}$ cm^{-3}) (see fig. 3.12 (a)) and a heavily-doped non-fully-depleted cell ($p = 3\times10^{15}$ cm^{-3}) (see fig. 3.12 (b)). The back-barrier height for both cells is varied. Fig. 3.12 (a) shows that the fully-depleted cell with a lower back barrier has a higher conduction-band barrier.

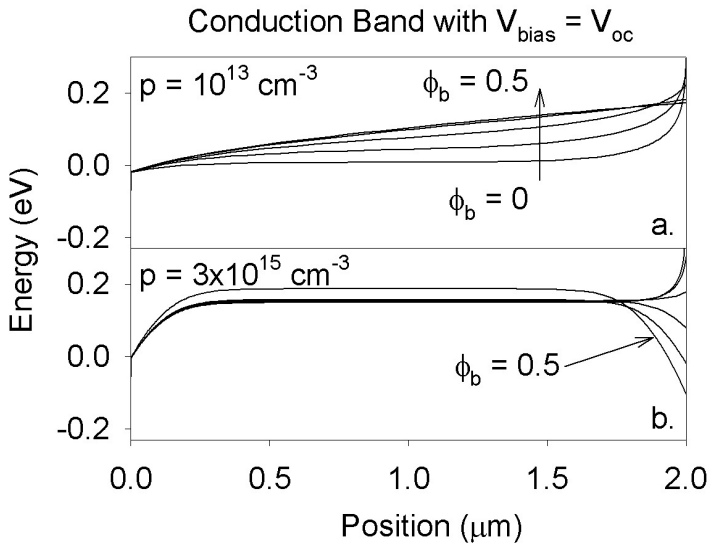

Fig. 3.12 Conduction bands with $V_{bias} = V_{oc}$, a range of back-barrier heights, as well as (a) $p = 10^{13}$ cm^{-3} and (b) $p = 3\times10^{15}$ cm^{-3}.

In fig. 3.13 (a), the calculated J-V curves corresponding to fig. 3.12 are shown, illustrating that this barrier serves as an electron reflector to improve V_{oc}. However, the sign and magnitude of the back barrier has minimal effect on the heavily-doped cell ($p = 3\times10^{15}$ cm^{-3}) due to its very thin depletion region at the back surface (see fig. 3.12 (b)). Fig. 3.13 (b) summarizes the effect of the thin reversed back barrier on V_{oc}. This also applies to the heavily-doped back surface mechanism. A large back barrier (0.5 eV), however, still has a negative effect on the cell with $p = 3\times10^{15}$ cm^{-3}.

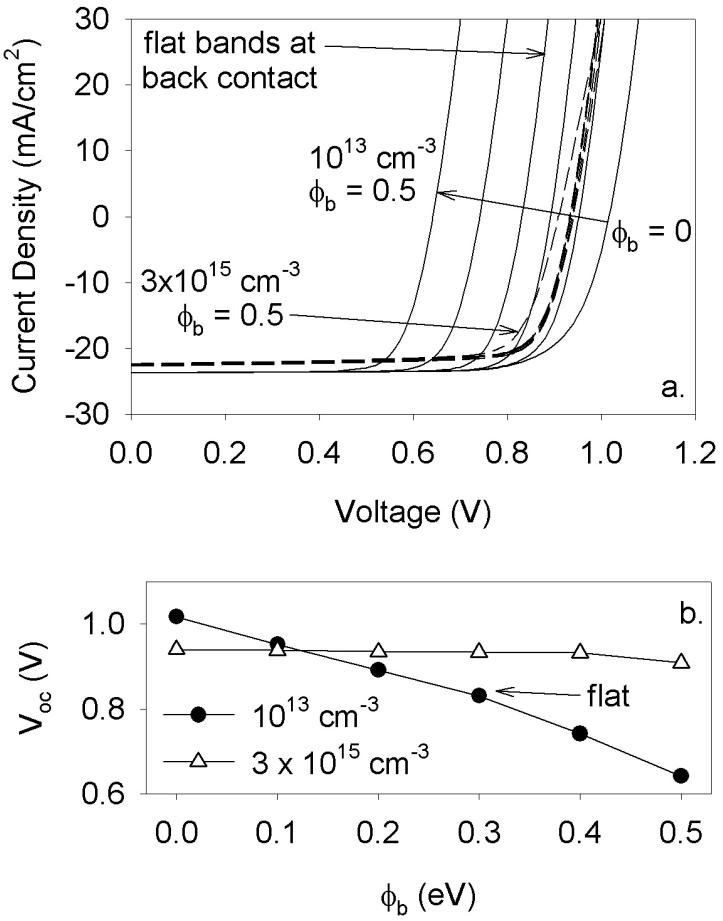

Fig. 3.13 (a) The calculated J-V curves with varied back-barrier heights for the two-carrier-density variation (solid lines for 10^{13} and dashed lines for 3×10^{15} cm^{-3}). (b) Calculated effect of the reversed back barrier on V_{oc}.

3.2.2.2 Heavily Doped Back Surface

For higher hole density near the back surface, the Fermi level will be closer to the top of the valence band, and a barrier in the conduction band will be formed at the back surface. The barrier height for this kind of electron reflector is quantified by the ratio of the carrier density of the electron-reflector layer to that of the bulk layer, or p_{ER}/p_{bulk}. Fig. 3.14 (a) shows the conduction bands of cells with a range of carrier density ratios. The calculated J-V curves corresponding to fig. 3.14 (a) are shown in fig. 3.14 (b). They

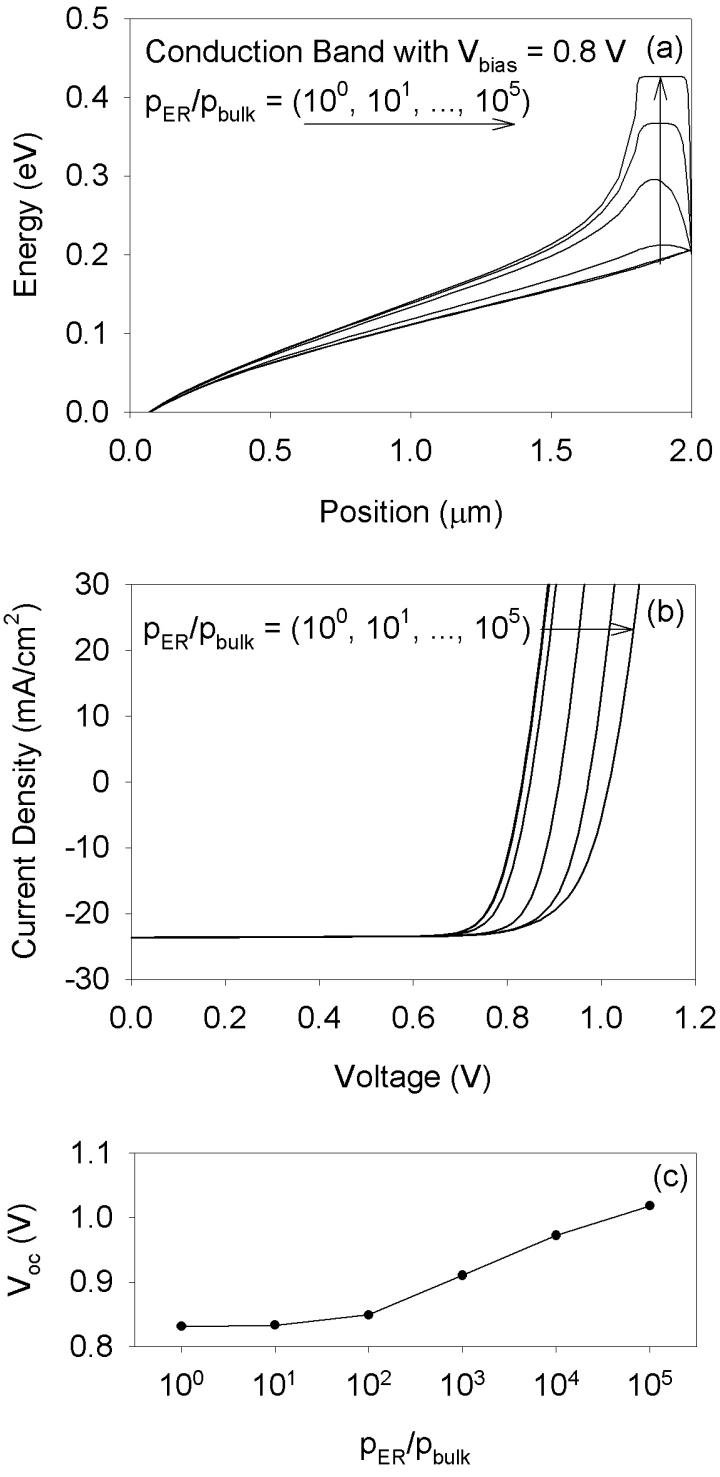

Fig. 3.14 (a) Conduction bands of cells with different p_{ER}/p_{bulk} at V_{bias} = 0.8 V. (b) Calculated corresponding J-V curves. (c) The calculated effect of p_{ER}/p_{bulk} on V_{oc}.

illustrate that this barrier also functions like an electron reflector. Fig. 3.14 (c) summarizes the effect on V_{oc}. However, the effectiveness of a depleted electron-reflector layer is likely to be limited for doping increases less than a factor of 100.

The thickness of the doping layer (d_{ER}) also affects the depletion of a cell. Fig. 3.15 (a) shows conduction bands of cells with different d_{ER} (50, 100, 200, 300, and 400 nm) for two conditions ($p_{bulk} = 10^{13}$ cm^{-3} with $p_{ER}/p_{bulk} = 10^3$ and $p_{ER}/p_{bulk} = 10^5$). The calculated effect is shown in fig. 3.15 (b).

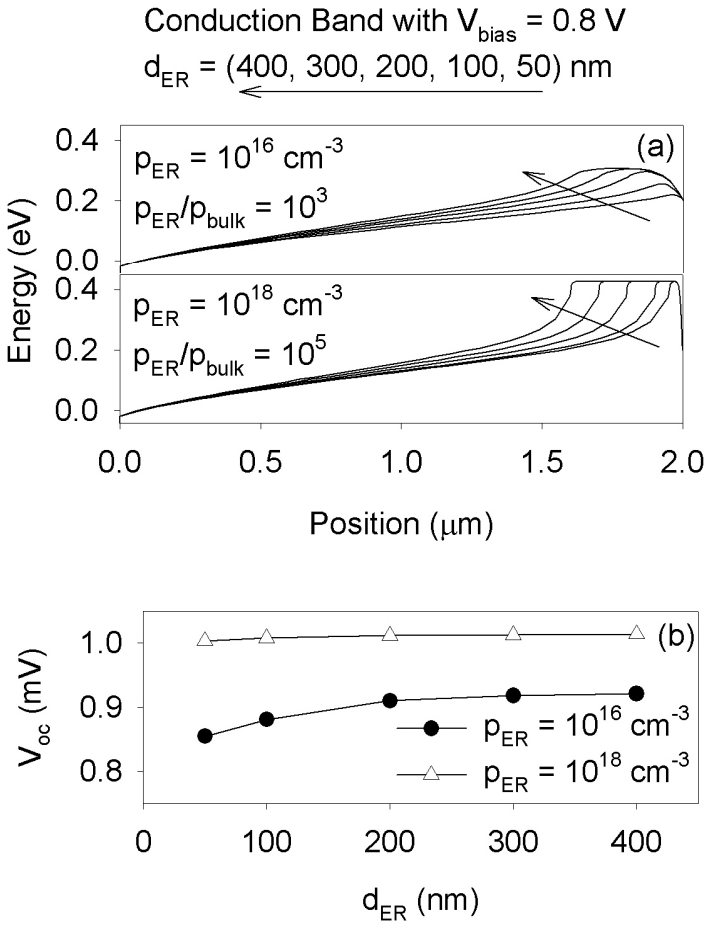

Fig. 3.15 (a) Conduction bands with a range of d_{ER} for two p_{ER}/p_{bulk} values (10^3 and 10^5 with $p_{bulk} = 10^{13}$ cm^{-3}). (b) The calculated effect of d_{ER} on V_{oc}.

To have an optimal effect, the carrier density and the thickness of the electron-reflector layer need to be chosen to prevent the depletion of the electron-reflector layer.

△ △ △ △ △ △ △ △ △ △ △ △ △ △ △

Four different mechanisms to create an electron reflector were introduced. In the next section, the contour plot will be used to find the condition for the optimal effect of the electron-reflector strategy.

3.3 Optimal Condition for Electron-Reflector Strategy

In this section, the optimal conditions for the electron-reflector strategy will be explored. A cell with a 1-ns lifetime and a 2-μm absorber layer is again used here. Fig. 3.16 shows contour plots of calculated parameters, including V_{oc}, J_{sc}, FF, and eff with varied carrier densities (10^{13}-10^{18} cm^{-3}) and reflector-barrier heights (0-0.4 eV). Each plot shows carrier density on the x-axis and electron-reflector barrier height on the y-axis.

The J_{sc} contour plot shows that the reflector barrier has little effect on $J_{sc.}$ Higher carrier density does lower J_{sc} due to a thinner depletion region for carrier collection. The other contour plots have odd patterns, primarily due to the kink shown in fig. 3.5.

The term "kink quadrant" denotes the quadrant where the kink occurs. Hence, the labels "no", "1^{st}", and "4^{th}" mean no kink, kink in the first quadrant, and kink in the fourth quadrant respectively. Fig. 3.17 shows the same contour plots with the kink-quadrant labels. Because the formation of a kink is continuous, the delineations are approximate. Fig. 3.17 shows that efficiency and V_{oc} increase with reflector barrier height in the no-kink quadrant where the cell is fully depleted at a specific carrier density. With

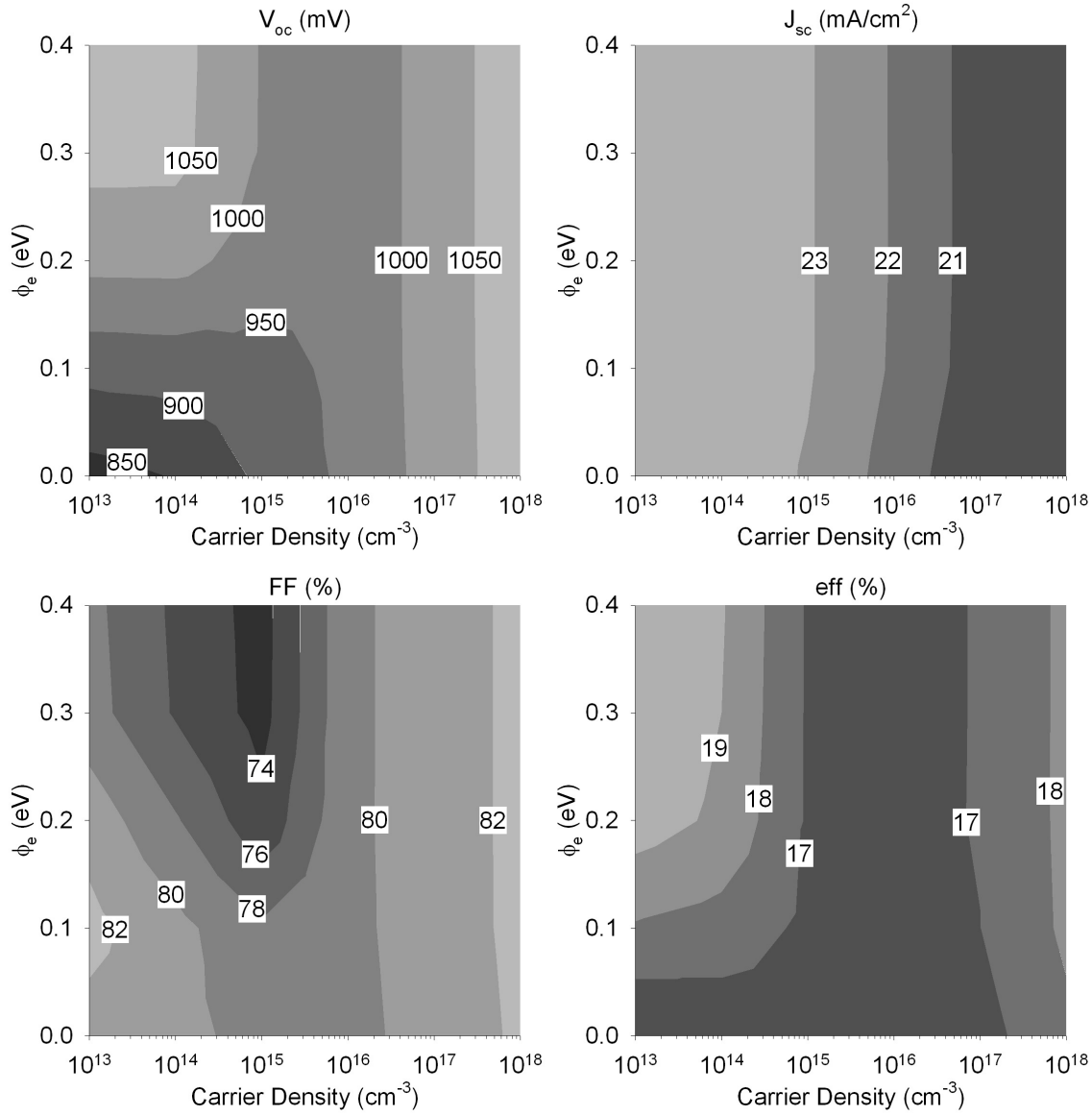

Fig. 3.16 Contour plots of calculated parameters (1-ns lifetime).

carrier densities above 10^{16} cm^{-3}, the reflector barrier height has little effect on parameters. In general, a 4th-quadrant kink degrades FF. For a cell thicker than 2 μm with lower carrier density, a lower reflector barrier may still have a kink due to its wider non-depleted region, where no built-in field can assist the carrier collection. For lower-lifetime (less than 1 ns) and non-fully-depleted cells (2 μm with hole density above 10^{14}

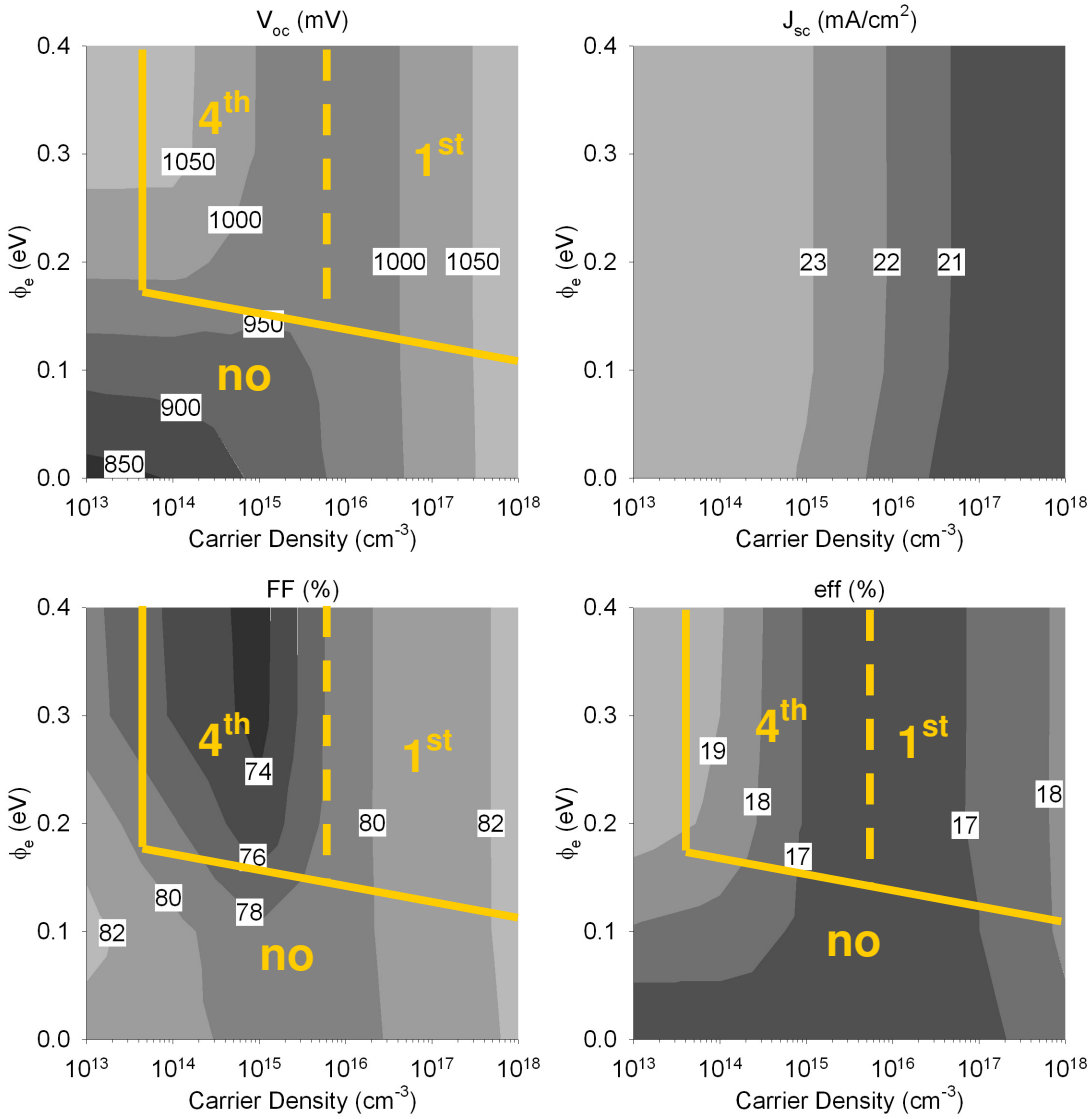

Fig. 3.17 Contour plots of calculated parameters with kink quadrant. (1-ns lifetime)

cm^{-3}), a kink is also possible with a lower electron-reflector barrier due to serious recombination in the non-depleted bulk region.

Fig. 3.18 shows additional contour plots with a range of lifetimes (0.01-100 ns) and reflector barrier heights (0-0.4 eV). Absorber thickness is fixed at 2 μm and current density at 10^{13} cm^{-3}, low enough that there will be no kink. Efficiency and V_{oc} increase

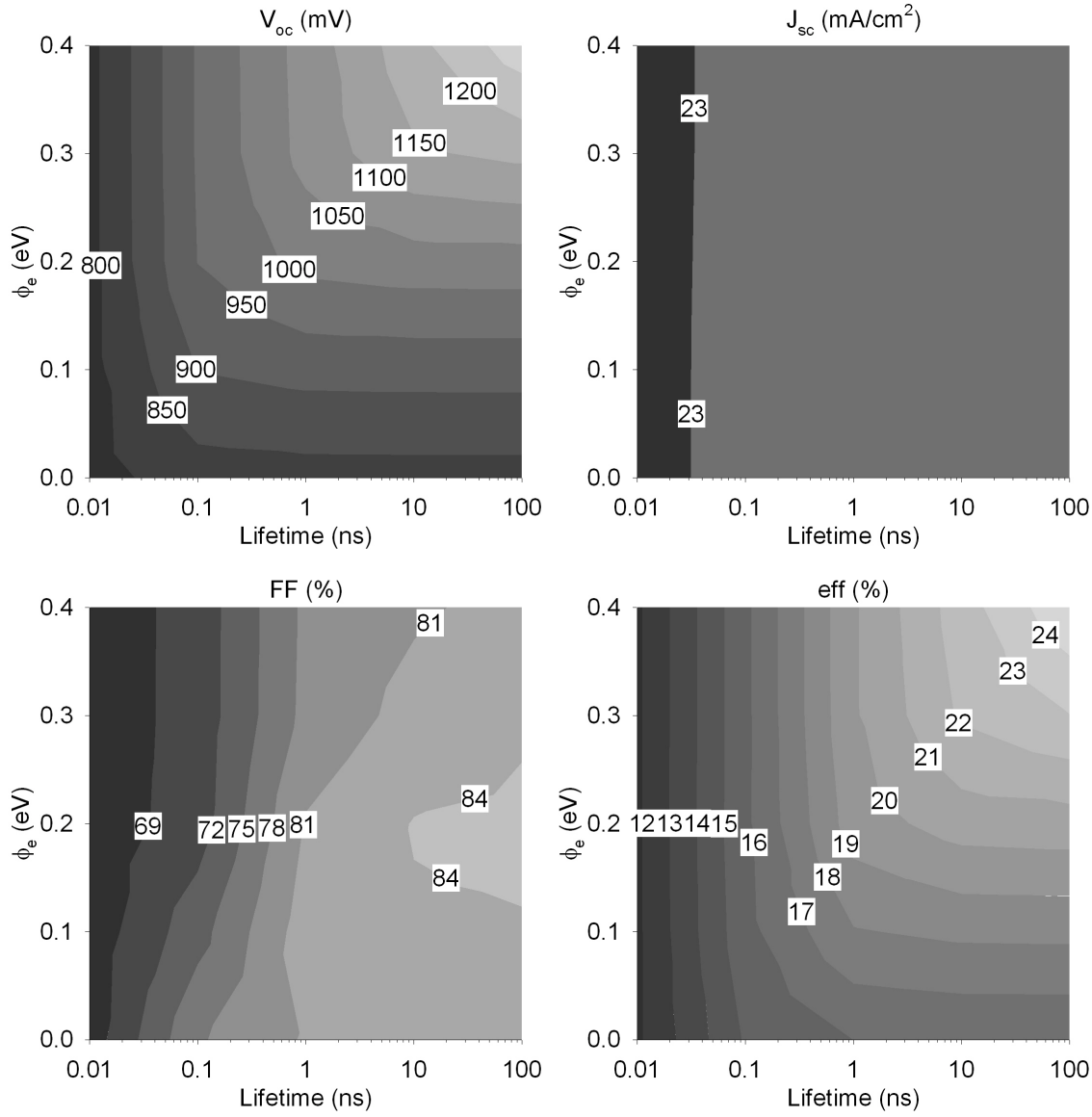

Fig. 3.18 Contour plots of calculated parameters (a 2-µm thickness, a 10^{13}-cm^{-3} carrier density).

with ϕ_e at longer lifetimes. In all cases, the reflector barrier has little effect on J_{sc}. When the lifetime is short, the reflector barrier has little effect on any of the parameters, because carriers recombine before they reach the back surface. Finally, a cell with a fixed 0.2-eV electron reflector leads to fig. 3.19, which shows contour plots with varied carrier densities (10^{13}-10^{18} cm^{-3}) and lifetimes (0.01-100 ns). The kink-quadrant notation is

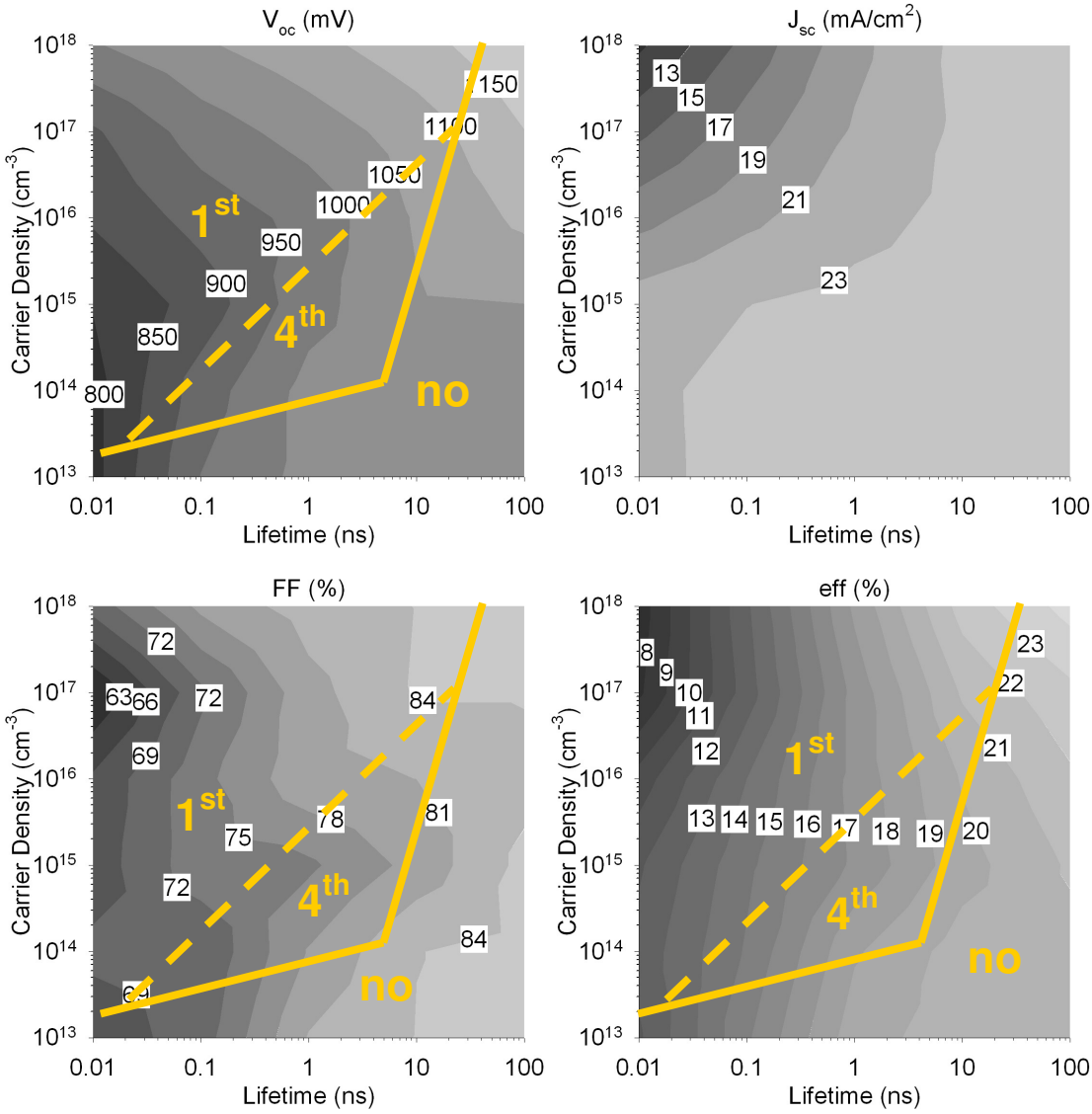

Fig. 3.19 Contour plots of calculated parameters (ϕ_e = 0.2 eV).

again applicable. Based on this figure, a reasonable long lifetime (1ns or above) and full depletion are required to have the optimal effect from the electron reflector.

The improvement of parameters, defined as the difference between parameters with and without a 0.2-eV electron reflector, is shown in fig. 3.20. Theoretically, an increase of 200 mV in voltage and 3% in efficiency is achievable by applying the

proposed electron-reflector strategy to cells currently available (a CdTe cell with a 1-ns lifetime, a 10^{13}-cm^{-3} carrier density, and a 2-μm absorber layer).

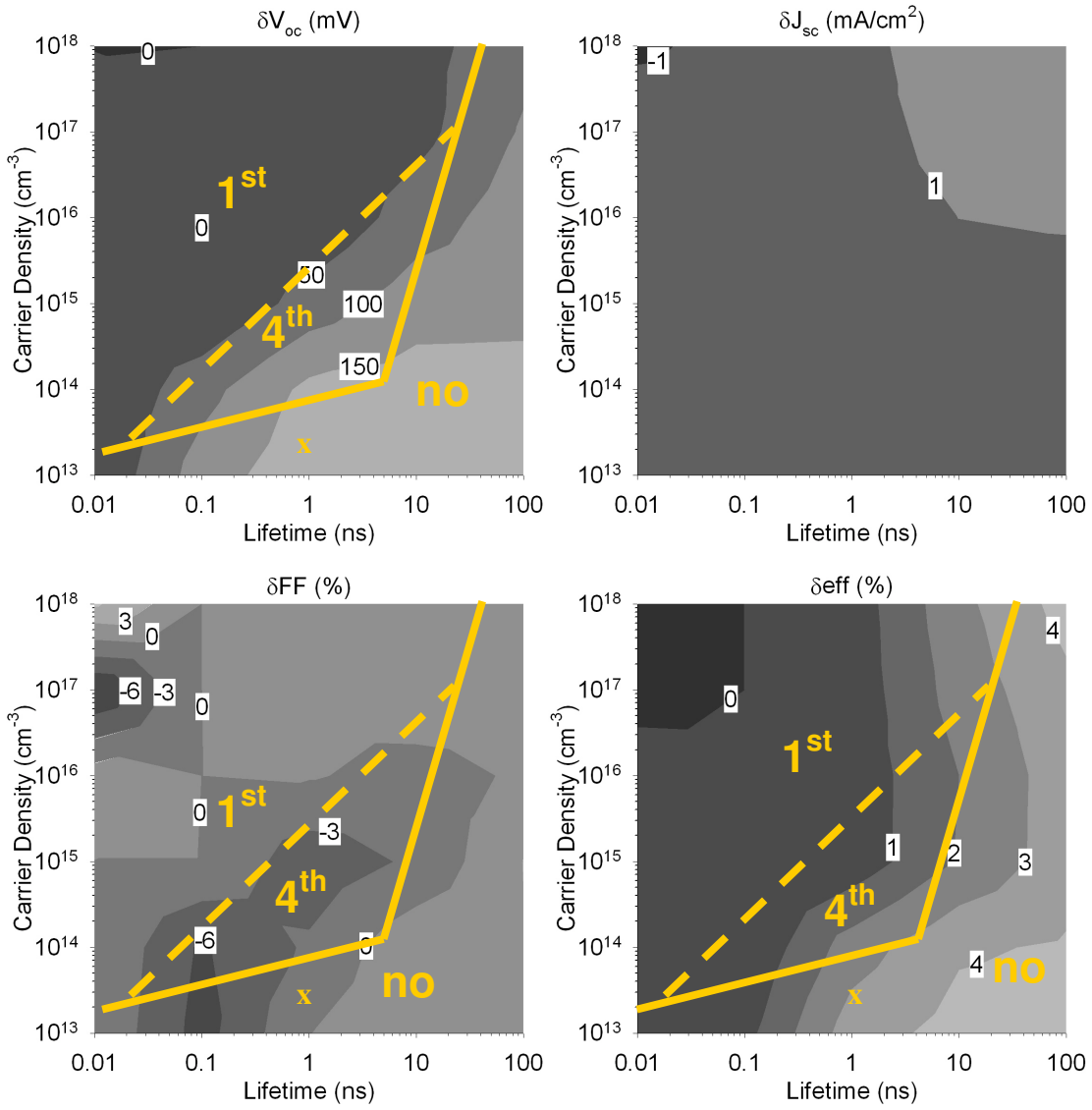

Fig. 3.20 Contour plots of improvement on calculated parameters (ϕ_e = 0.2 eV). "x" makes the best point currently practical.

3.4 Related Issues

In the previous sections, the mechanisms and the optimal condition of the electron-reflector strategy were investigated. After an electron-reflector layer is created,

however, an additional interface is formed. Possible interfacial-recombination and valence-band-offset issues will be investigated in this section.

3.4.1 Interfacial Recombination

After an electron-reflector layer is deposited on the back side of the CdTe absorber layer, an additional interface is formed between the two layers. Fig. 3.21 shows the band diagram with the formed reflector interface at V_{bias} = 0.8 V. This interfacial recombination is quantified by the recombination velocity S_i. A baseline cell with S_b = 10^7 cm/s is used. Fig. 3.22 shows the calculated J-V curves with different values of S_i and ϕ_e. The J-V curve of a cell with a 0.2-eV electron reflector and S_i = 10^7 cm/s is similar to that of a cell with no electron reflector. That means that if interfacial recombination is as serious as back-surface recombination, the deposited electron-reflector layer only shifts the problem due to back-surface recombination to interfacial recombination. Therefore, a good-quality reflector interface is required for the electron-reflector strategy.

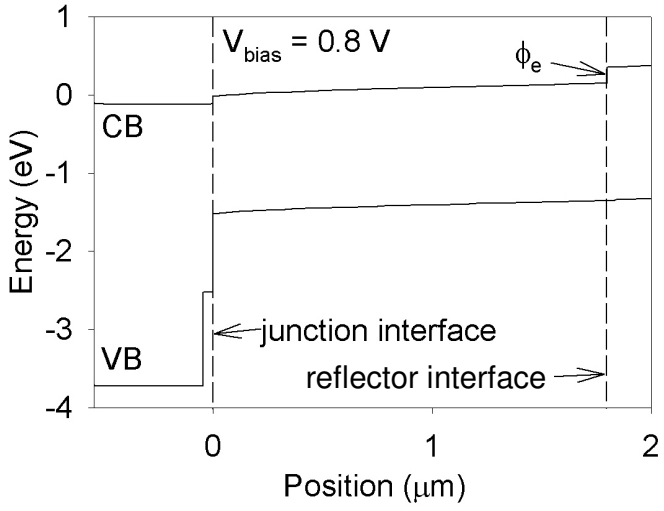

Fig. 3.21 Band diagram with reflector interface indicated.

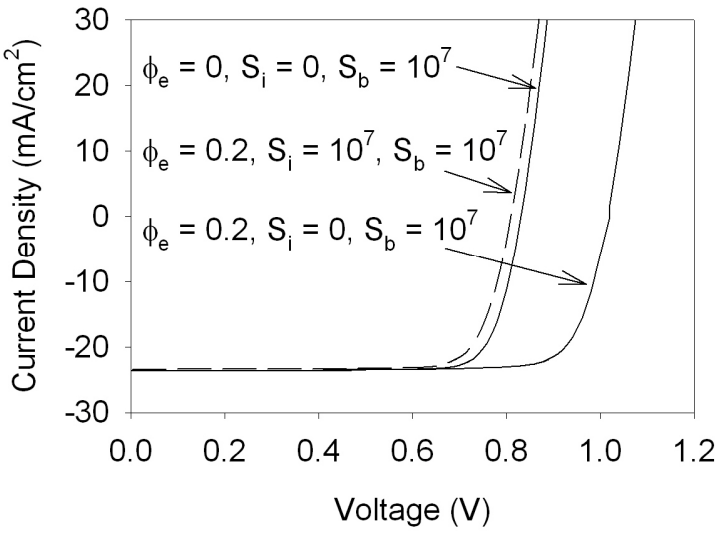

Fig. 3.22 Calculated J-V curves with different values of S_b, S_i, and ϕ_e.

3.4.2 Valence-Band Offset

Fig. 3.23 shows the calculated band diagram of a CdTe cell with a ZnTe electron-reflector layer, which can create a 0.8-eV barrier height. A 0.2-eV electron-reflector barrier can be created by alloy CdZnTe with 25% in Zn composition. A 0.1-eV valence-

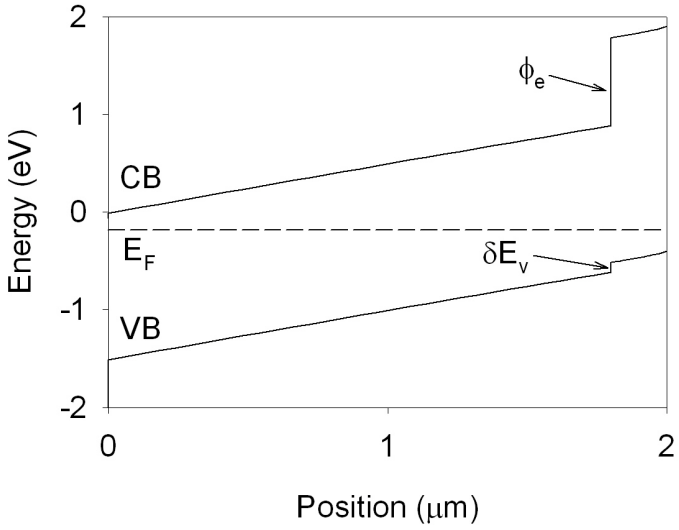

Fig 3.23 Band diagram with valence-band offset indicated.

band offset has been found for the ZnTe/CdTe interface [19]. The valence-band offset is quantified by the parameter δE_V, which is indicated in fig. 3.23. With $\delta E_V \leqq 0.1$ eV, the valence-band offset has little effect on the cell performance. Therefore, the valence-band offset at the CdTe/CdZnTe interface should be negligible in the electron-reflector strategy.

3.5 Chapter Summary

In this chapter, four different mechanisms of electron reflector are investigated, and we learn that full depletion and reasonable lifetime (1 ns or above) are required to have the optimal effect from the electron reflector.

Chapter 4

Interaction of Mechanisms

Different mechanisms to create an electron reflector were introduced in chapter three. In this chapter, pairs of mechanisms will be combined to see whether an additional improvement is possible. Then the mechanisms will be compared to see which one is the best mechanism for CdTe thin-film solar cells to create an electron reflector.

4.1 Combination

Here, the combination of any two of the four mechanisms will be investigated. Due to the thin depletion region of the reversed back barrier at a heavily-doped back surface, and the similarity between an expanded-band-gap layer and the bulk-band-gap reduction, we consider only these three combinations:

4.1.1 Expanded-Band-Gap Layer plus Bulk-Band-Gap Reduction

4.1.2 Expanded-Band-Gap Layer plus Reversed Back Barrier

4.1.3 Expanded-Band-Gap Layer plus Heavily-Doped Back Surface

4.1.1 Expanded-Band-Gap Layer plus Bulk-Band-Gap Reduction

In the first case, an expanded-band-gap layer and a bulk-band-gap reduction are applied to the CdTe baseline model to see whether there is an additional improvement. Parameters of the baseline model are d_{abs} = 2 μm, p = 10^{13} cm^{-3}, and a 1-ns lifetime. Fig. 4.1 shows the contour plots of calculated parameters with varied ϕ_e (0-0.4 eV) and varied Eg_{bulk} (1.2-1.5 eV). Fig. 4.2 is similar with the lifetime increased to 10 ns. Each plot

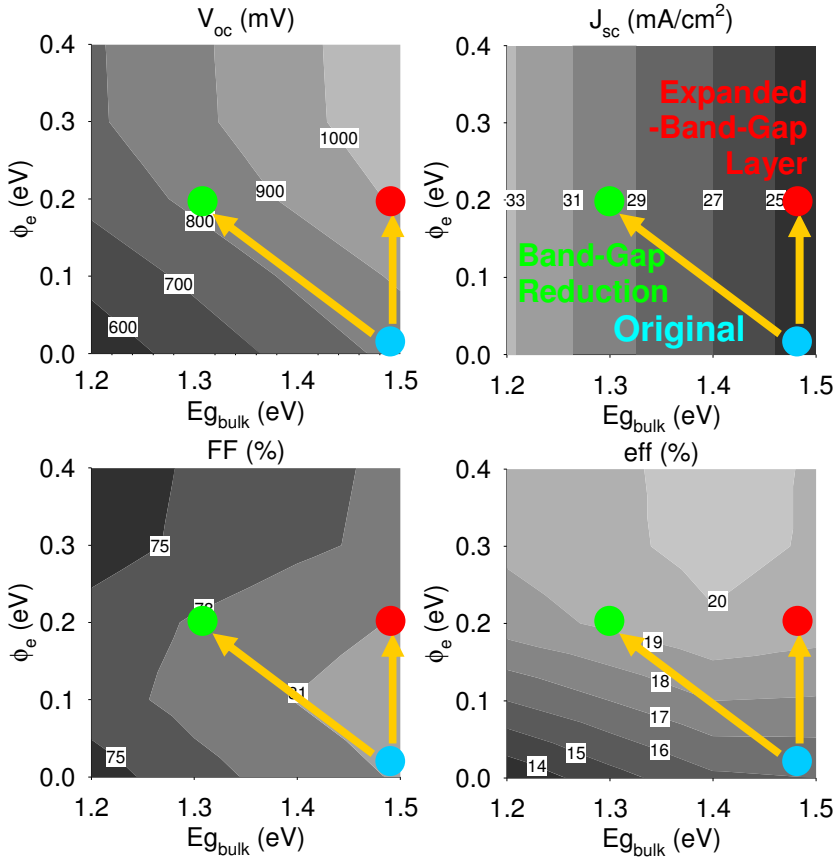

Fig. 4.1 Contour plots of calculated parameters with a 1-ns lifetime. $Eg_{ER} = Eg_{bulk} + \phi_e$. Blue, red, and green dots represent a baseline cell without electron reflector, a cell with a 0.2-eV expanded-band-gap layer, and a cell with a 0.2-eV bulk-band-gap reduction respectively.

shows Eg_{bulk} on the x-axis and ϕ_e on the y-axis. Eg_{ER} is the addition of Eg_{bulk} and ϕ_e. In the contour plots, blue, red, and green dots represent a baseline cell without electron reflector, a cell with a 0.2-eV expanded-band-gap layer, and a cell with a 0.2-eV bulk-band-gap reduction respectively. The J_{sc} contour plot shows the shift of absorption spectrum due to a lower Eg_{bulk} raises J_{sc}. The V_{oc} contour plot shows that V_{oc} increases with Eg_{ER} ($Eg_{ER} = Eg_{bulk} + \phi_e$) when ϕ_e is below 0.2 eV. The combination of mechanisms with $\phi_e = 0.2$ eV is in the region between red and green dots. It increases both V_{oc} and J_{sc}, yet it has no additional improvement in efficiency. The efficiency contour plot in fig. 4.1

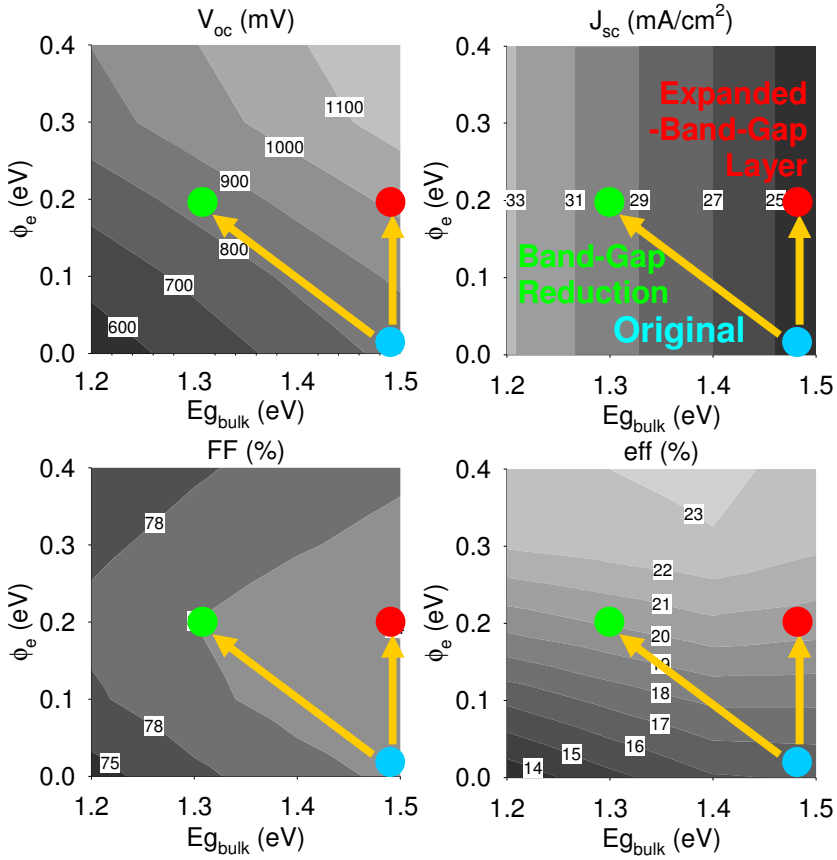

Fig. 4.2 Contour plots of calculated parameters with a 10-ns lifetime. Blue, red, and green dots represent a baseline cell without electron reflector, a cell with a 0.2-eV expanded-band-gap layer, and a cell with a 0.2-eV bulk-band-gap reduction respectively.

shows a 0.2-eV reflector barrier created with either an expanded-band-gap layer or bulk-band-gap reduction can make the efficiency exceed 19%. However, the improvement of efficiency is saturating as the reflector barrier is above 0.2-eV with a 1-ns lifetime. Fig. 4.2 along with the higher lifetime gives a very similar result with approximately a 1% increase in absolute efficiency compared to the lower lifetime.

4.1.2 Expanded-Band-Gap Layer plus Reversed Back Barrier

In this simulation, the combination of an expanded-band-gap layer and a reversed back barrier, which is explored in section 3.2.2.1, is investigated. Fig. 4.3 shows the contour plots of calculated parameters, including Voc, FF, and eff, with varied ϕ_e (0-0.4 eV) and varied ϕ_b (0-0.5 eV). Note that a 0.3-eV baseline for the back barrier is a flat band for the carrier density used. Below 0.3 eV, the hole barrier is gone and an electron barrier appears. Each plot shows ϕ_b on the x-axis and ϕ_e on the y-axis. J_{sc} is around 23.7 mA/cm^2 for all conditions. The plots show that a lower back-contact barrier requires a

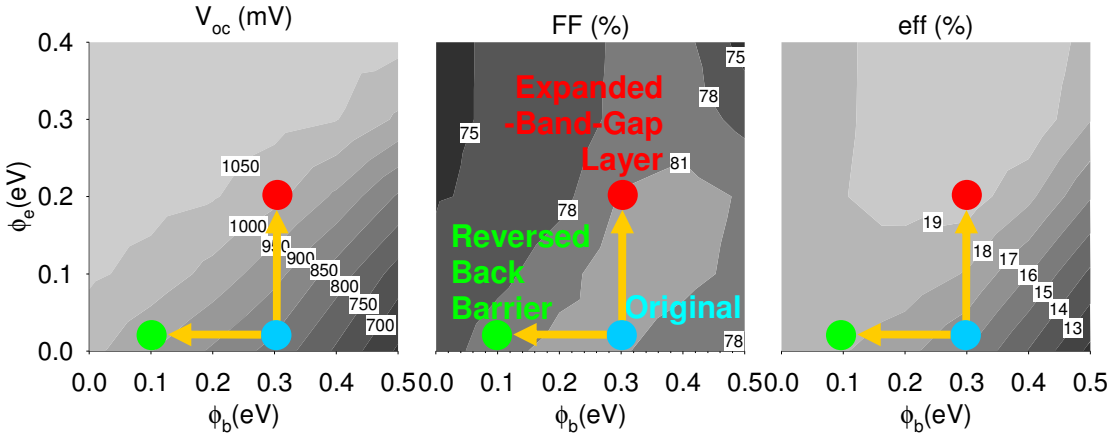

Fig. 4.3 Contour plots of calculated parameters. Blue, red, and green dots represent a baseline cell without electron reflector, a cell with a 0.2-eV expanded-band-gap layer, and a cell with a 0.1-eV reversed back barrier respectively.

smaller electron-reflector barrier for a similar effect on voltage and efficiency. In the plot, blue, red, and green dots represent a baseline cell, a cell with a 0.2-eV electron reflector, and a cell with a 0.1-eV reversed back barrier respectively. We can see that a 0.2-eV reflector barrier with a flat back-contact barrier (ϕ_b = 0.3 eV) can already can reach 19% efficiency, and the combination of a reversed back barrier and the expanded-band-gap layer does not show an additional improvement on efficiency. This situation is likely unphysical in any case, since the problem has always been to reduce the hole barrier to a manageable value.

4.1.3 Expanded-Band-Gap Layer plus Heavily-Doped Back Surface

In this case, an expanded-band-gap layer and a heavily-doped back surface are applied to a baseline cell. The carrier density in the bulk part of the absorber layer (p_{bulk}) is fixed at 10^{13} cm^{-3}. Fig. 4.4 shows the contour plots of calculated parameters with varied

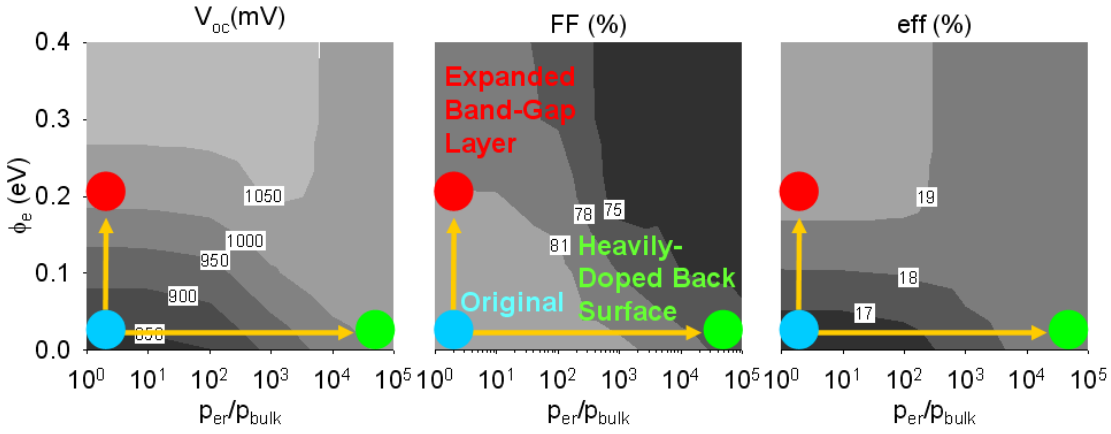

Fig. 4.4 Contour plots of calculated parameters (a 1-ns lifetime, p_{bulk} = 10^{13} cm^{-3}). Blue, red, and green dots represent a baseline cell without electron reflector, a cell with a 0.2-eV expanded-band-gap layer, and a cell with a heavily-doped back surface at p_{ER}/p_{bulk} = 10^5 respectively.

ϕ_e (0-0.4 eV) and varied p_{ER}/p_{bulk} (10^0-10^5). The x-axis of the contour plot shows p_{ER}/p_{bulk}, and the y-axis shows ϕ_e. J_{sc} is around 23.7 mA/cm^2 for all conditions. The contour plot shows that there is a trade-off between V_{oc} and FF, which will limit the effect. This combination also does not show an additional improvement on efficiency.

△ △ △ △ △ △ △ △ △ △ △ △ △ △ △

From fig. 4.1.1-4.1.4, we can conclude:

- Qualitatively similar results from different strategies.
- Little or no gain from combinations.

In the next section, different mechanisms will be compared to find the best mechanism for CdTe thin-film solar cells to create an electron reflector.

4.2 Comparison

In this section, three mechanisms to increase voltage, the expanded-band-gap layer, the reversed back-contact barrier, and the heavily-doped back surface, will be compared. Again, bulk-band-gap reduction is not considered separately, because its effect is very similar to expanded-band-gap layer.

Fig. 4.5 summarizes the effect of different mechanisms on voltage, fill factor, and efficiency. The results for mechanisms are plotted against its corresponding parameter (ϕ_e for expanded-band-gap layer, ϕ_b for reversed back barrier, and p_{ER}/p_{bulk} for heavily-doped back surface). Fig. 4.5 (a) shows that V_{oc} varies relatively linearly with ϕ_e, ϕ_b, or

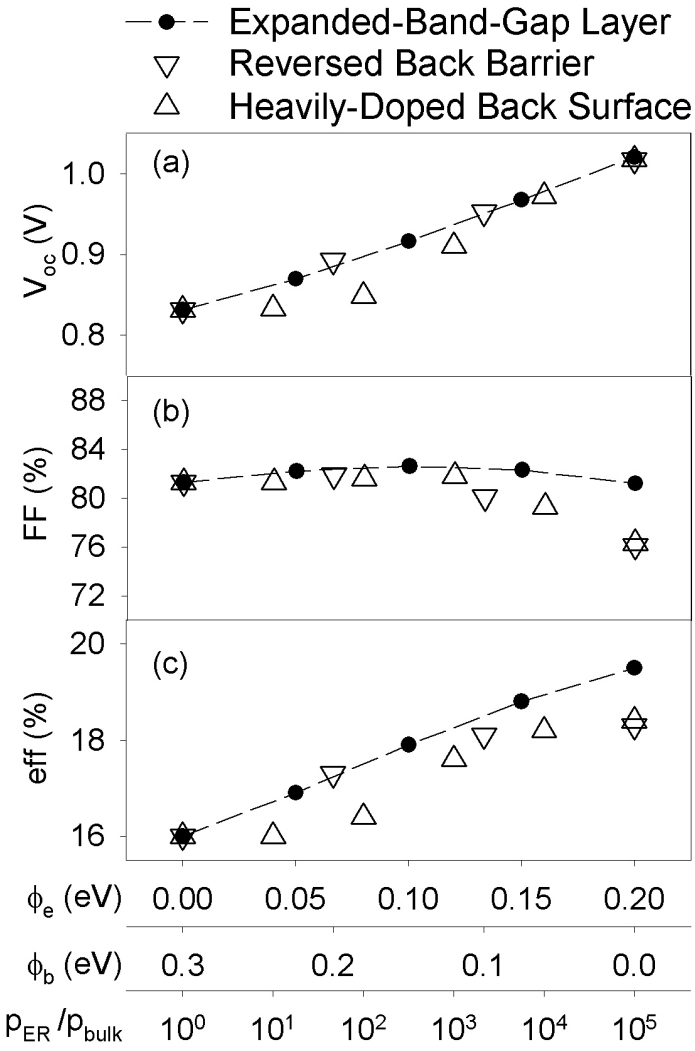

Fig. 4.5 Comparison of the three electron-reflector mechanisms. Fits shown are for the expanded-band-gap strategy.

p_{ER}/p_{bulk}, and that V_{oc} can exceed 1 V with any of the three mechanisms. Fig. 4.5 (b) shows that fill factor changes slightly with parameters, but starts to decrease when the voltage increase is above 100 mV for a reversed back barrier and a heavily-doped back surface. Fig. 4.5 (c) shows that the efficiency increases relatively linearly with parameters, but saturates when the fill factor begins to decrease for band-bending mechanisms. J_{sc} is not plotted because the electron-reflector strategy has little effect on J_{sc}. Among these

mechanisms in fig. 4.5, that of the expanded band gap is the only one to raise V_{oc} above 1 V without compromising the FF. The improvement in V_{oc} and the maintenance of the FF make the expanded-band-gap approach more likely to be efficient than the other two mechanisms. The predicted efficiency improvement is approximately 50% larger. Furthermore, it is highly unlikely that a p-type CdTe will have a reversed back barrier due to its very high work function, and p-type CdTe is not easily heavily doped because it is generally heavily compensated. Consequently, the expanded-band-gap layer is probably more practical than the others.

Fig. 4.6 shows that the calculated conduction bands of cells with different electron-reflector mechanisms at open-circuit voltage. One can see that cells with different types of electron-reflector barriers should all result in a voltage increase approaching 200 mV, but the details of the conduction-band diagrams are quite different. Moreover, the barrier height of the expanded-band-gap layer is a constant with variation in external bias.

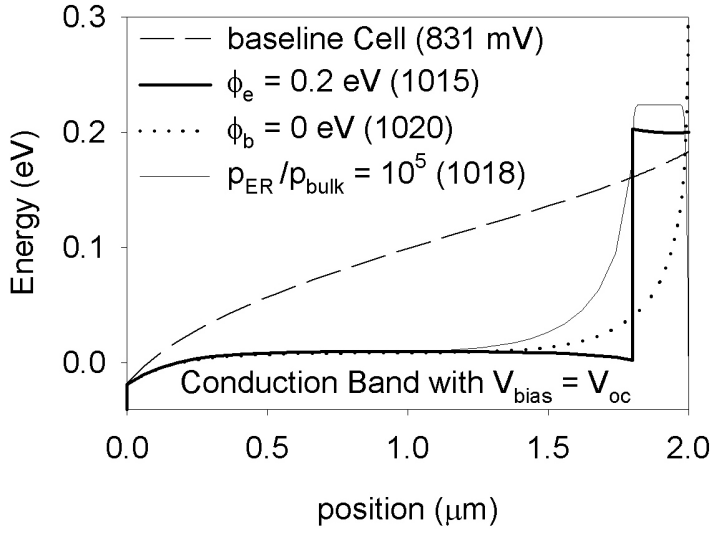

Fig. 4.6 Conduction bands of cells with different mechanisms at open-circuit voltage.

4.3 Chapter Summary

Based on the comparison of the electron-barrier mechanisms above, the expanded-band-gap strategy should be more efficient and practical than a reversed back barrier or a heavily-doped back surface because the expanded band gap can improve V_{oc} without compromising FF. Furthermore, the other strategies are limited by the nature of CdTe, and there is no additional improvement from any combination of mechanisms.

Chapter 5

Electron-Reflector Applications

In this chapter, two applications of the electron-reflector strategy for CdTe solar cells will be investigated with one-dimensional numerical simulation. One is based on the record-CdTe-cell baseline model to investigate possibilities for a breakthrough in the efficiency. The other is based on the thin-CdTe-cell baseline model to see how an electron reflector could affect the efficiency of thin CdTe cells.

5.1 Record CdTe Solar Cells

Fig. 5.1 summarizes the reported solar-cell parameters of record cells since 1991. In 1991, a thin-film CdTe solar cell with 13.4% efficiency (by T.L. Chu, S.S. Chu, et al at USF) was reported [20]. Record cells were then reported as having an efficiency of 14.6% in 1992 (T.L. Chu, S.S. Chu, et al at USF [21]), 15.8% in 1993 (C. Ferekides, J. Britt, et al at USF [22, 23]), 16% in 1997 (Hideaki Ohyama, et al at Matsushita Battery Industrial Co., Ltd. [24]), and 16.5% in 2001 (X. Wu, et al at NREL [5]). The record efficiency increased with improved J_{sc} from 1991 to 1993, but since then improvement

has slowed. No new record has been made for about ten years since the 16.5% cell was reported.

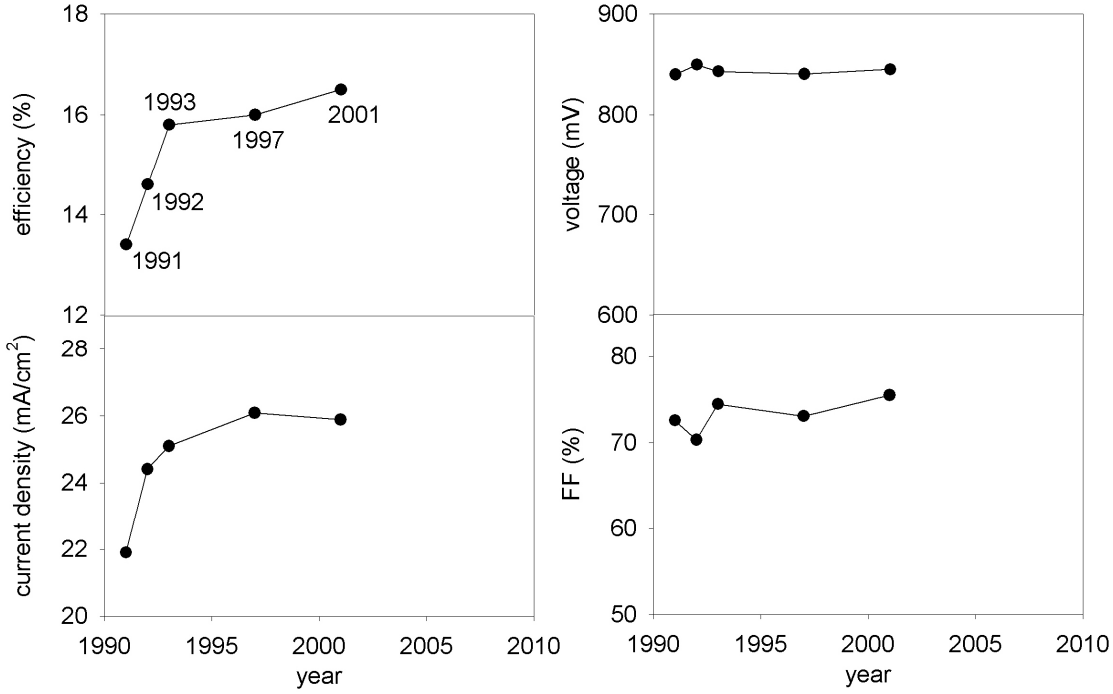

Fig. 5.1 Reported solar-cell parameters of record CdTe thin-film solar cells

To have a breakthrough in efficiency of CdTe thin-film solar cells, research should focus on the V_{oc}, which is well below what is expected for its band gap (Eg = 1.5 eV). In this section, the electron-reflector strategy is numerically applied to the record-CdTe-cell baseline to investigate possibilities for a breakthrough in the efficiency.

5.1.1 The Record CdTe Cell

In the work to follow, a baseline cell is built to numerically match the record-efficiency CdTe cell. This record-cell baseline has a 1-ns carrier lifetime, a 1×10^{14}-cm^{-3} hole density, a 10-μm absorber layer, and a flat back-barrier band. Fig. 5.2 shows that the

J-V curve of the record-cell baseline matches the reproduced J-V curve of the record cell well [5].

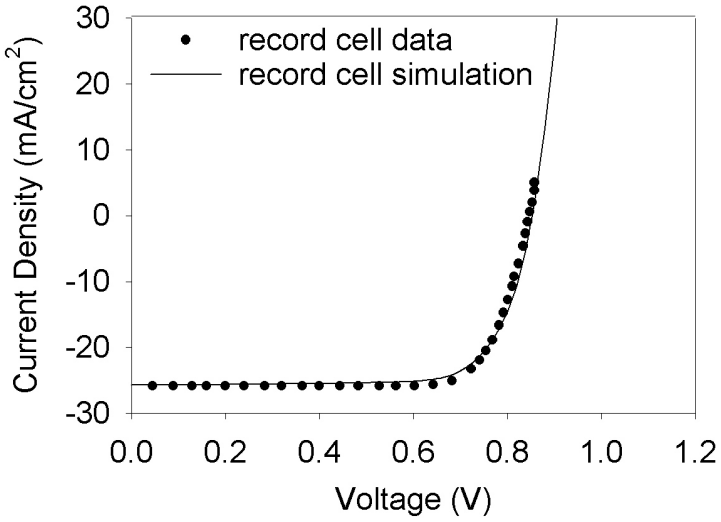

Fig. 5.2 J-V curves of the record-CdTe-cell baseline and the simulated baseline for the record CdTe cell.

Fig. 5.3 shows contour plots on calculated solar-cell parameters of the baseline record cell with variations in absorber thickness (0.4-10 μm) and hole density (10^{13}-2×10^{14} cm^{-3}). Each plot shows the thickness on the x-axis and the hole density on the y-axis. The red dots in the contour plots are used to represent the record cell. The reported parameters (V_{oc} = 845 mV, J_{sc} = 25.9 mA/cm^2, FF = 75.5%, eff = 16.5%) of the record cell are shown on the contour plots by those dots.

5.1.2 Record Cell with Electron and Optical Reflection

Based on the previous chapters the expanded-band-gap layer was found to be the most efficient and practical way to create an electron reflector on CdTe thin-film solar cells, and a 0.2-eV electron reflector should increase the V_{oc}. Therefore, a 0.2-eV

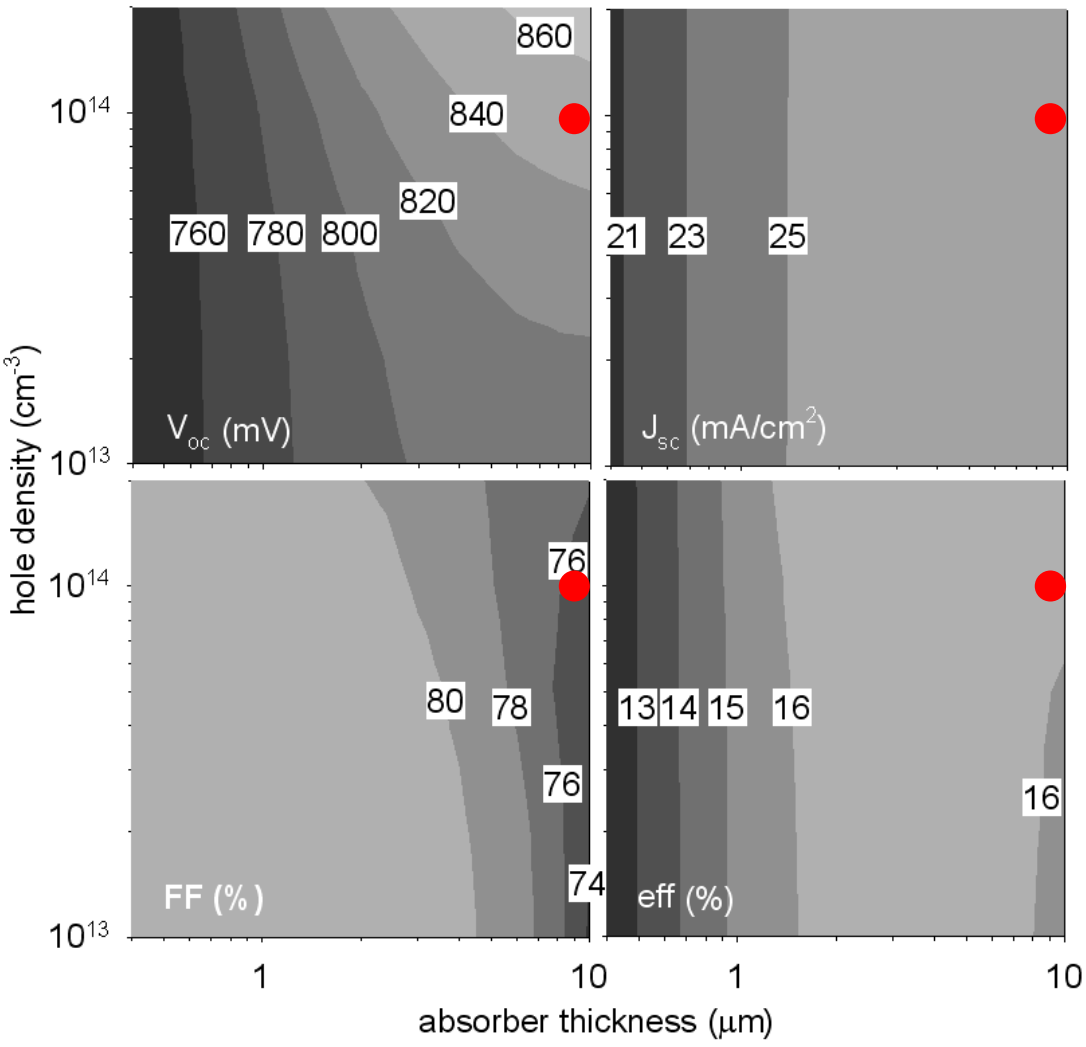

Fig. 5.3 Contour plots on calculated solar-cell parameters of the record-CdTe-cell baseline with variations in carrier density (10^{13}-2×10^{14} cm^{-3}) and absorber thickness (0.4-10 μm). The red dots represent the record CdTe cell.

expanded-band-gap layer is chosen to be applied to the record-CdTe-cell baseline numerically.

A thin layer of metal such as gold or copper at the back surface between the metal contact and the absorber layer should reflect much of the transmitted long-wavelength light back through the absorber layer. Therefore, the long-wavelength light would have a

second pass to be absorbed, and in turn the photon collection should be increased. This strategy to increase the photon collection is referred to as optical back reflection. The optical back reflectivity R_b is the qualifying parameter.

Fig. 5.4, with the same axes as fig. 5.3, shows the contour plots on the calculated solar-cell parameters of a CdTe cell with a 0.2-eV electron reflector and 20% optical

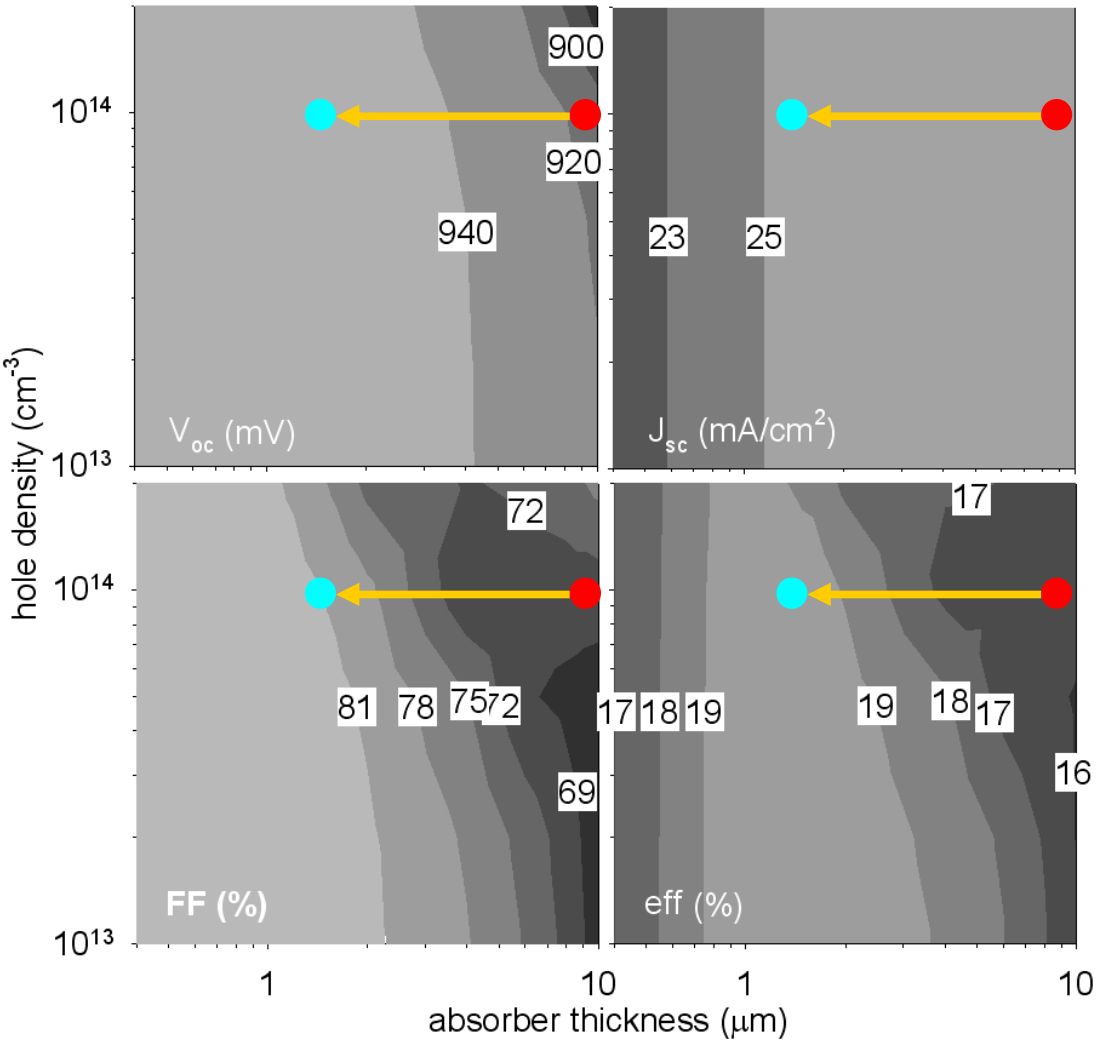

Fig. 5.4 Contour plots of the calculated solar-cell parameters for a CdTe cell with a 0.2-eV electron reflector and 20% optical back reflection. Red dots represent a record-cell baseline model with a 0.2-eV electron reflector and 20% optical back reflection, and blue dots represent a thinned record cell baseline model with a 0.2-eV electron reflector and 20% optical back reflection.

back reflection. The red dots represent the record-cell baseline model with a 0.2-eV electron reflector and 20% optical back reflection. Fig. 5.5 is similar with the optical back reflection increased to 100%. In fig. 5.4, the calculated efficiency with the two strategies reaches 19% for the fully depleted cells with an absorber layer thicker than 0.6 μm. V_{oc} is improved under all conditions, particularly for the fully depleted cells. J_{sc} is improved by optical back reflection when the absorber thickness is less than 2 μm, and the FF changes slightly. However, the benefit from the two strategies has little value for the 10-μm record cell due to its lack of full depletion and its already complete absorption. To have the optimal effect from the electron reflector, thinning cells to below two microns is required, and at the same time, the optical back reflection to compensate for the incomplete-absorption loss becomes important. The arrows in the plots represent thinning cells, and blue dots represent the thinned record-cell baseline with a 0.2-eV electron

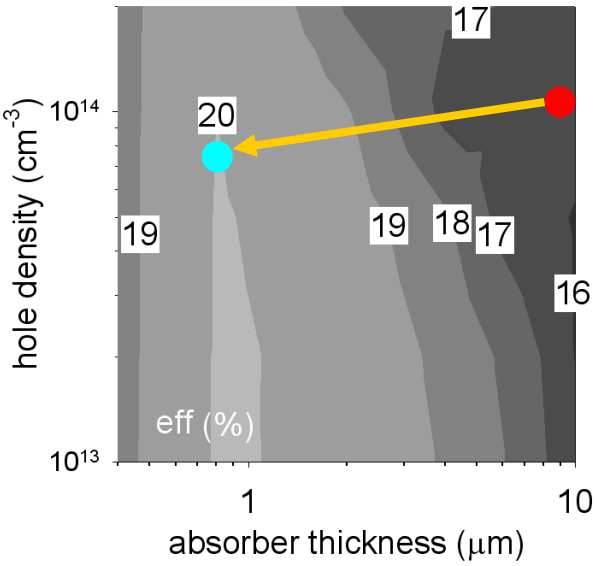

Fig. 5.5 Contour plots of the calculated efficiency with a 0.2-eV electron reflector and 100% optical back reflection. Red dot represents a record-cell baseline model with a 0.2-eV electron reflector and 100% optical back reflection, and blue dot the thinned record cell with a 0.2-eV electron reflector and 100% optical back reflection.

reflector and 20% optical back reflection (fig. 5.4), or 100% optical back reflection (fig. 5.5). In the latter case, the incomplete-absorption loss will be well compensated for by the doubled optical absorption path. Fig. 5.5 shows that the efficiency with a 0.2-eV electron reflector and 100% optical back reflection should achieve 20% near 1-μm thickness (blue dot).

5.1.3 Summary

Fig. 5.6 shows the calculated J-V curves for the record-cell baseline (dashed line), a 1-μm record-cell baseline with ϕ_e = 0.2 eV, and a 1-μm record-cell baseline with ϕ_e = 0.2 eV and R_b = 100%. With ϕ_e = 0.2 eV and a 1-μm absorber layer, the V_{oc} of the record-cell baseline is increased by about 100 mV. Moreover, with ϕ_e = 0.2 eV and R_b = 100% applied to the 1-μm record-cell baseline, a 20% efficiency should be possible. Without changing the cell quality, thinning cells to near one micron is a practical way to profit from electron reflector and optical back reflection.

5.2 Thin CdTe Solar Cells

Thinning solar cells without compromising their performance should lead to lower-cost PV devices, because thinner cells require less fabrication time and less material. The University of Toledo has in fact successfully fabricated a 0.3-μm CdTe solar cell with 6.8% efficiency and a 0.5-μm cell with 9.7% efficiency [25]. The thin CdTe solar cell with a typical carrier density should be fully depleted, and hence, the back-surface recombination is a primary limitation to the performance. Moreover,

incomplete optical absorption with a thin absorber layer will cause a current loss. The two strategies to minimize the loss due to back-surface recombination and incomplete absorption are now compared to the experimental data in ref. [25].

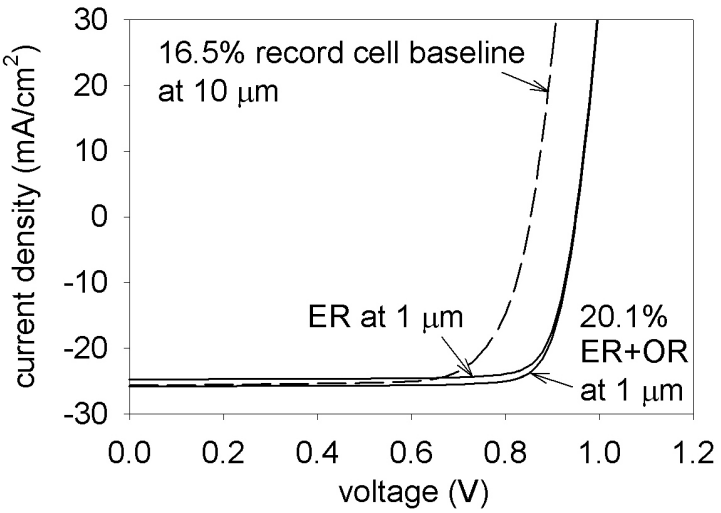

Fig. 5.6 J-V curves for the record CdTe cell (dashed line), cell thinned to 1 μm with a 0.2-eV electron reflector (ER), and thinned cell with 0.2-eV electron reflector (ER) and 100% optical back reflection (OR).

5.2.1 Thin-Cell Baseline

A thin, but reasonable, cell (J_{sc} = 23.7 mA/cm^2, V_{oc} = 870 mV, FF = 80.2%, R_s = 1 Ω·cm^2, G = 0.2 mS/cm^2, and efficiency = 16.6%) is defined here for the thin-CdTe-cell baseline. This baseline cell has a 1-ns carrier lifetime, a 2×10^{14}-cm^{-3} hole density, a 2-μm absorber layer, a thin CdS layer, and a flat back-contact barrier.

Fig. 5.7 shows calculated quantum efficiency (QE) curves for a range of thicknesses (0.4, 0.8, and 1.2 μm). A 100% optical back reflection is applied to a 0.4-μm cell. The dashed line shows that a 0.4-μm cell with R_b = 100% will have a similar QE curve to the 0.8-μm cell without optical back reflection due to the doubled length of the

optical absorption path. For thin cells, the optical back reflection can significantly reduce the incomplete-absorption loss.

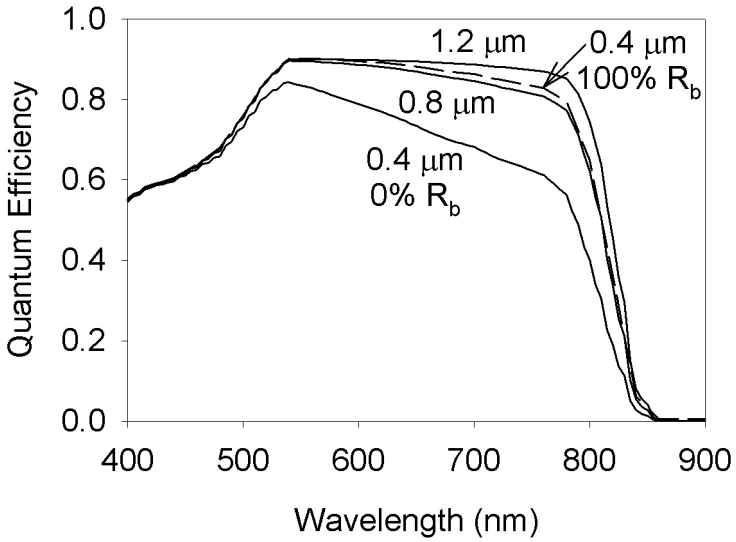

Fig. 5.7 Calculated QE curves of cells with R_b = 0% for three thicknesses. R_b = 100% only shown for 0.4 μm.

Fig. 5.8 compares the calculated solar-cell parameters with the experimental ones from reference [25] for cells with a range of thicknesses. The calculated and experimental efficiencies show a similar decrease, but there are differences with the individual parameters. When the cell is thinner, the back-surface recombination becomes more

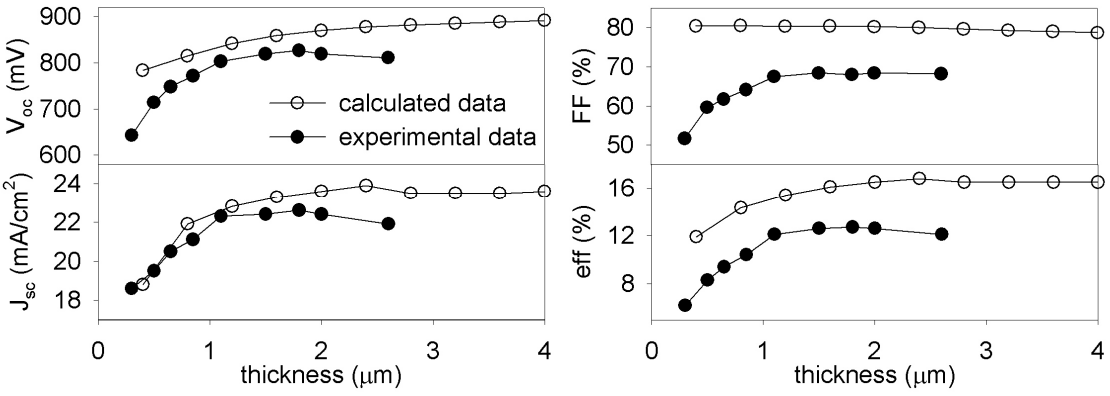

Fig. 5.8 calculated (open circles) and experimental (filled circles) solar-cell parameters of cells with varied thicknesses.

serious. Therefore, the open-circuit voltage and the current density decrease at smaller thicknesses, as seen with both the simulated and experimental cases. Moreover, incomplete absorption loss degrades current density at thicknesses below 2 μm. With fill factor (FF), however, the experimental and simulated curves show a significant difference. Thickness has little effect on the calculated fill factor, but the lifetimes in reference [25] were quite likely reduced with the smaller thickness. Similarly, the experimental voltage decreases more than that predicted by the calculation.

5.2.2 Thin Cells with Electron and Optical Reflection

Fig. 5.9 shows calculated parameters of cells with a range of thicknesses and varied electron-reflector barrier heights of 0, 0.1, and 0.2 eV. The green dots are the same as the calculated dots in fig. 5.8. The calculated parameters of a cell with ϕ_e = 0.2 eV and R_b = 100%, including J_{sc} and efficiency, are also shown. The band diagram of a thick cell is shown as a reference for the depletion width of this baseline setting. The baseline cell is also marked for reference.

In fig. 5.9, V_{oc} is significantly enhanced by electron reflector at all thicknesses, and FF falls at larger thicknesses when an electron-reflector cell is no longer fully depleted. The electron reflector has little effect on J_{sc}. Hence, a maximum in efficiency versus thickness is predicted. With a 0.2-eV electron reflector, the highest-efficiency electron-reflector CdTe cell without optical back reflection is calculated to have a 1.2-um absorber layer (V_{oc} = 990 mV, J_{sc} = 23 mA/cm^2, FF = 80%, eff = 18%). On the other hand, thinner cells benefit from the optical back reflection on J_{sc}. With 100% optical back reflection, the optimal calculated thickness is 0.8 um (Voc = 990 mV, Jsc = 23 mA/cm^2,

FF = 83%, eff = 19%). A realistic optical reflector is in between 0 and 100%. Therefore, the suggested optimal thickness for thin CdTe solar cell with an electron reflector is one micron. Theoretically, competitive CdTe cell performance at thickness as thin as 0.4 um should be possible with electron reflector and optical back reflection (see fig. 5.9).

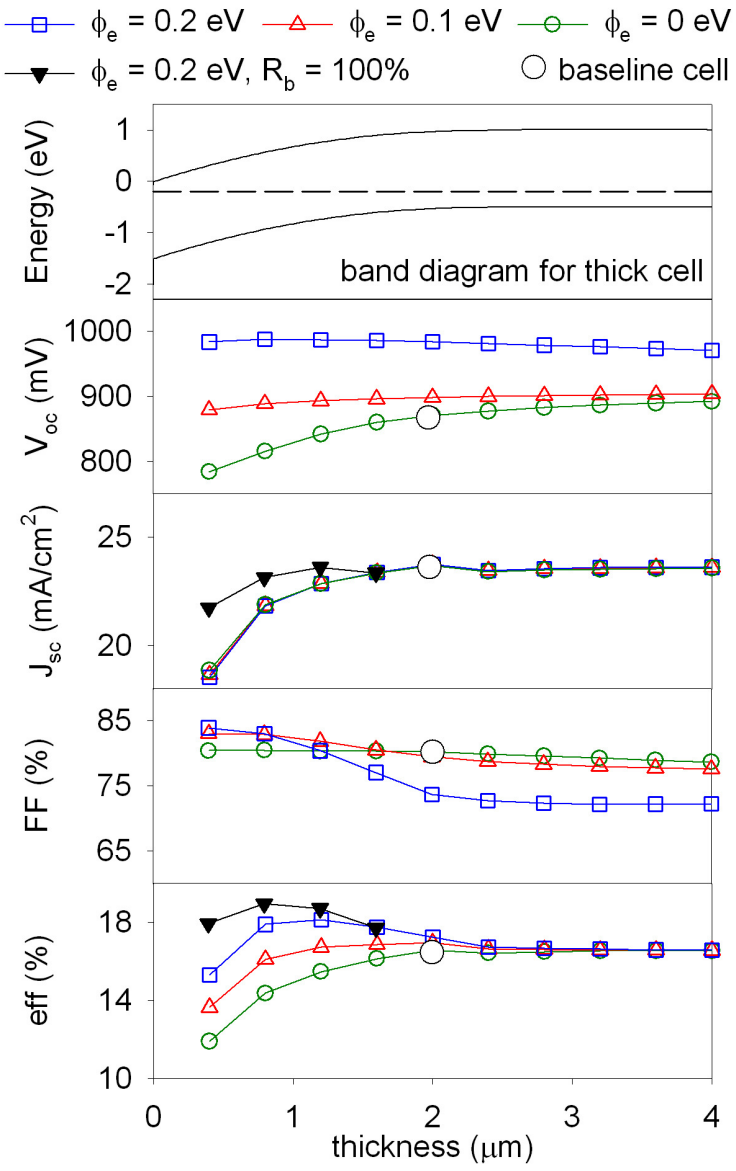

Fig. 5.9 Band diagram of a thick CdTe cell and calculated parameters of cells with a range of thicknesses and electron reflector barrier heights. Parameters for cell with ϕ_e = 0.2 and R_b = 100% also shown. Baseline cell marked with circle.

5.3 Chapter Summary

Theoretically, cell efficiency above 19% should be achievable with a 0.2-eV electron reflector, 20% optical back reflection, a 1-μm absorber layer, a 10^{14}-cm^{-3} hole density, and a 1-ns lifetime. Efficiency above 20% should be possible if one can achieve large optical back reflection. Moreover, the highest-efficiency thin CdTe cell with a 50-nm electron reflector layer should have a CdTe thickness of about one micron. Competitive CdTe cell performance at a thickness as thin as 0.4 um should be possible.

Chapter 6

Experimental Results

A set of CdTe thin-film solar cells were fabricated to test the electron-reflector strategy. A ZnTe layer was deposited at the back surface of the CdTe cell as an electron-reflector layer. The CdTe cells with the ZnTe back layer appeared to show a higher open-circuit voltage, but other aspects of the J-V curves were inferior, and the sample set was too small to be conclusive.

CdTe cells which were used for a preliminary test of the electron-reflector strategy were fabricated with CSS (close-space-sublimation) continuous in-line process in the Materials Engineering Laboratory (MEL) at Colorado State. The continuous in-line process suitable for manufacturing CdTe solar cells has been the core of Walajabad Sampath's lab [26]. This in-line process is performed in one chamber with a moderate operating pressure (40-mTorr N_2). Cells with reasonable performance were obtained and good stability was verified [27-30].

Fig 6.1 shows the schematic of the in-line process. There are nine stops inside the chamber. Each stop has two heat reservoirs (top and bottom). The temperatures of top and bottom reservoirs are controlled as fabrication parameters. The bottom temperature is

used to control the deposition rate and the top temperature the substrate conditions. When the system is in operation, cleaned superstrates are manually loaded on the automated conveyor. Every two minutes, the conveyor belt will transport each superstrate forward to the next operation stop, and a cell with all processes done will emerge from the output AVA (air to vacuum, then to air) seal. AVA seals keep the vacuum chamber in high vacuum, such that superstrates can be continuously loaded into the chamber and exit without venting the chamber. All the deposition and treatment are done in the vacuum chamber.

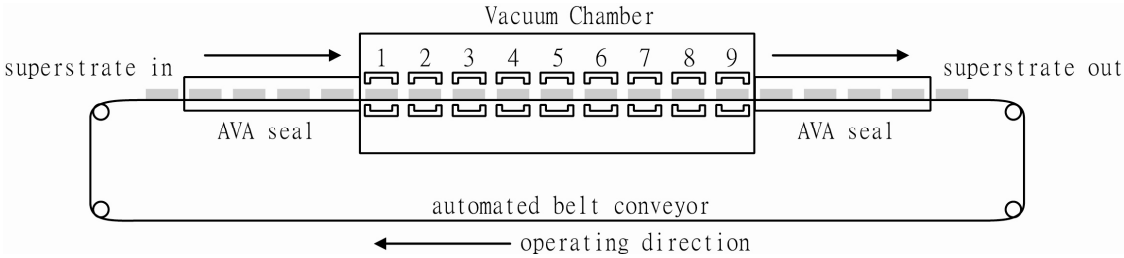

Fig. 6.1 Schematic of the in-line process in MEL at CSU. Stops inside the chamber:

1. **heating module**
2. **CdS deposition**
3. **CdTe deposition**
4. **$CdCl_2$ treatment**
5. **annealing**
6. **stripping**
7. **space**
8. **Cu treatment**
9. **annealing**

After the superstrate is moved through the AVA seal to the vacuum chamber, the superstrate is heated to operating temperature in stop 1. CdS and CdTe are deposited with the CSS technique, which has been well investigated for CdTe deposition [22, 31], in

stops 2 and 3 respectively. Post-deposition treatments are performed from stop 4 to 9. A common and apparently necessary step for high-efficiency CdTe solar cells is the chlorine treatment. In stops 4 and 5, the $CdCl_2$ treatment is performed. The possible effects of $CdCl_2$ treatment are activating carriers, grain recrystallization, and interdiffusion [32, 33]. Stop 6 has a much lower temperature than stop 5 - by about 200K. Therefore, excess $CdCl_2$ will be stripped off by resubliming. Stop 7 is an extra space without heater or source. In stop 8, Cu is deposited to heavily dope the back surface, so that a tunneling contact can be achieved. Stop 9 is used to anneal the last step.

After the CdTe cells exit off the chamber, a graphite/nickel paste is sprayed to the deposition as the metal back contact. Then each superstrate will be cut to fifteen pieces. Finally, a sand blaster is used to delineate individual cells. The schematic of this cell definition is shown in fig. 6.2. Cells fabricated in this process with reasonably high efficiency are obtained. The cell labeled CSU 249-37-4b, which means that this cell is from the position labeled 4b of the superstrate labeled 37 that was fabricated in run 249 at CSU, was characterized. Fig. 6.3 shows the J-V curve of CSU 249-37-4b (J_{sc} = 21.9 mA/cm^2, V_{oc} = 783 mV, FF = 71.7%, R_s = 1.5 ohm – cm^2, G = 0.45 mS/cm^2, eff = 12.3%), which has fairly typical photovoltaic properties.

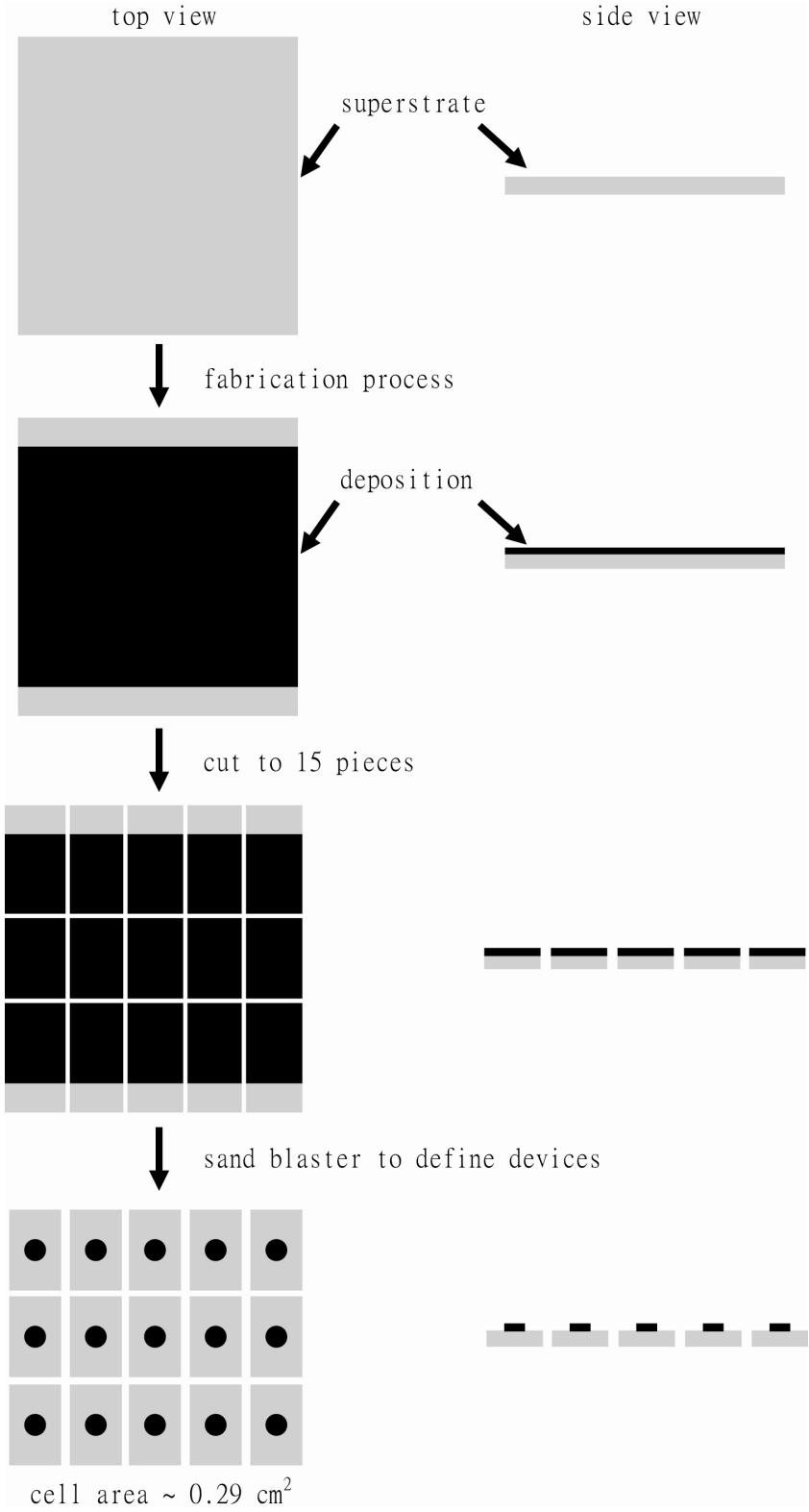

Fig 6.2 The schematic of the cell definition.

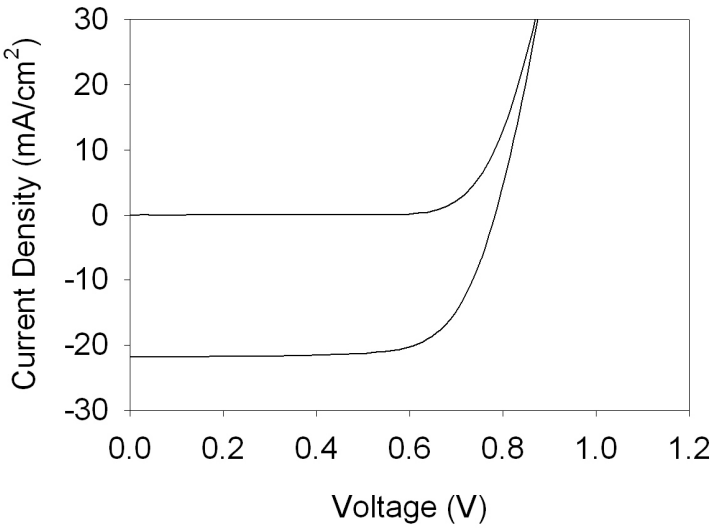

Fig 6.3 The J-V curve of CdTe thin-film solar cell CSU 249-37-4b.

To test the electron-reflector strategy experimentally, cell CSU 269-32-3 with a CdS/CdTe/ZnTe(source temperature at 630 °C)/metal-contact(C, Ni) configuration was fabricated. We split the fabrication process of this cell into two runs. In the first run, superstrate 269-32 went through stops 1 to 3, and then the CdTe source in stop 3 was replaced by the ZnTe source. In the second run, superstrate 269-32 went through stops 3 to 9. The proceeding process was the same. Fig 6.4 shows J-V curves of the typical cell CSU 249-37-4b (V_{oc} = 783 mV), and a ZnTe-back-layer cell CSU 269-32-3 (V_{oc} = 800 mV). Based on fig. 6.4, the CdTe cell with a ZnTe back layer has a slightly higher open-circuit voltage. However, the other parameters of CSU 269-32-3 were inferior, primarily because the process for this configuration was not optimized. The second run also showed that CdTe cells with a ZnTe back layer had a higher open-circuit voltage, but other aspects of the J-V curves were inferior, and the sample set was too small to be conclusive.

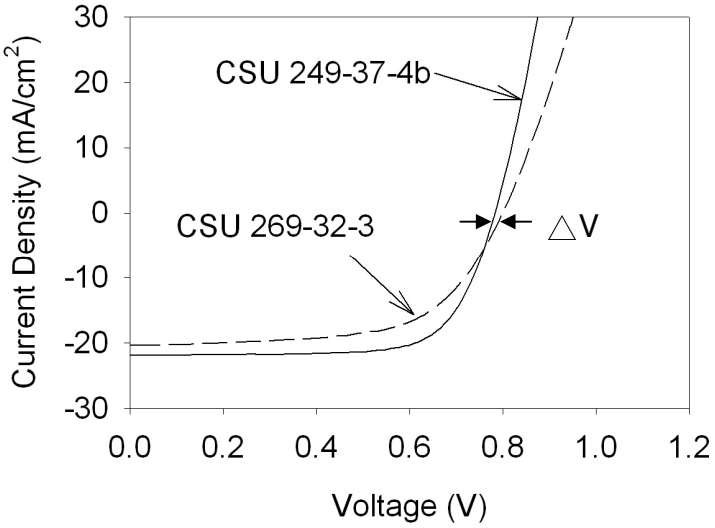

Fig 6.4 J-V curves of a typical cell CSU 249-37-4b (V_{oc} = 783 mV) and a ZnTe-back-layer cell CSU 269-32-3 (V_{oc} = 800 mV).

Chapter 7

Summary

7.1 Motivation

The CdTe thin-film solar cell has a large absorption coefficient, and its band gap is a good match to the solar spectrum, so it has high theoretical efficiency. Moreover, large-area panels can be fabricated economically. In fact, the largest photovoltaic company in the world, First Solar, uses CdTe for the absorber layer of its cells. All these features make the CdTe thin-film solar cell a potential large-scale alternative energy source. However, its record efficiency (16.5%) is much less than its theoretical maximal efficiency (29%), primarily because its open-circuit voltage (0.845 V) is well below what is expected for its 1.5-eV band gap. The electron reflector, which is a strategy to improve the open-circuit voltage without changing the cell quality, has the possibility of making a breakthrough in the efficiency of CdTe thin-film solar cells. This thesis gives a comprehensive investigation on the electron-reflector strategy with one-dimensional numerical simulation as the investigation approach.

7.2 Electron Reflector for CdTe Thin-Film Solar Cells

An electron reflector is a conduction-band barrier to electrons reaching the back solar-cell surface, which can reduce the back-surface recombination, especially at forward bias. There are two types of mechanisms to create an electron reflector. The first type of mechanism is an expanded band gap. For this mechanism, the band gap of the electron-reflector layer is larger than the band gap of the bulk part of the absorber layer. Either an expanded-band-gap layer or a band-gap reduction over most of the bulk can create an expanded band gap near the back. The former increases the open-circuit voltage, and the latter increases the short-circuit current. The second type of electron reflector is band bending. Either a reversed back barrier or a heavily-doped back surface can create an electron reflector by band bending.

Investigation shows that the expanded-band-gap layer should be more efficient and practical than a reversed back barrier or a heavily-doped back surface. Moreover, there is no additional improvement from any combination of mechanisms. Therefore, an expanded-band-gap layer is recommended for CdTe thin-film solar cells. Theoretically, an increase of 200 mV in voltage and 3% in absolute efficiency is achievable for a 2-μm CdTe cell with a 10^{13}-cm^{-3} hole density, a 1-ns lifetime, and a 0.2-eV electron reflector. To have the optimal effect of an electron reflector, a reasonable lifetime (1 ns or above) and full depletion are required. A good-quality interface between the p-type CdTe layer and the electron-reflector layer is required, or else the deposited electron-reflector layer simply shifts the loss caused by the back-surface recombination to the interfacial recombination. ZnTe or CdZnTe should be a good material for the electron-reflector barrier since the valence-band offset at CdTe/ZnTe interface is negligible and the band

expansion is almost exclusively in the conduction band. Preliminary experimental evidence has in fact shown that CdTe cells with a ZnTe back layer have a slightly higher open-circuit voltage.

7.3 Applications

In this thesis, the electron-reflector strategy is specifically applied to CdTe record- and thin- cell baseline models. The electron reflector should be particularly beneficial for cells with thicknesses below two microns when the CdTe absorber layer is fully depleted at a typical carrier density, because the back-surface recombination is a primary limitation to the performance of fully depleted cells. Cells with a thickness below two microns, and especially below one micron, can additionally also benefit from the optical back reflection.

If an electron reflector and optical back reflection were applied to the record-CdTe-cell baseline model, which is quite thick, there would be little improvement in the record cell's performance. To have the optimal effect from the two strategies, thinning cells to one micron for full depletion is required. Based on the calculation performed, more than 19% efficiency is achievable with a 0.2-eV electron reflector, a 1-μm absorber layer, a 10^{14}-cm^{-3} hole density, a 1-ns lifetime, and a 20% optical back reflection. Moreover, 20% efficiency is possible with 100% optical back reflection. Theoretically, the best calculated thin CdTe cell with a 50-nm electron reflector layer should have an absorber layer about one micron (efficiency: above 18%) and a competitive CdTe cell performance at thickness as thin as 0.4 um should be possible.

7.4 Chapter Summary

The theoretical frame of the electron-reflector strategy has been built. The future work should focus on the quantitative experimental investigation. This work should in particular focus on:

1. Optimizing the fabrication process of a CdTe solar cell with an electron reflector.
2. Determining the electron-reflector barrier height.
3. Testing the simulation results.

No record CdTe cells have been reported for almost ten years, since the 16.5%-efficiency record cell was reported. Based on this dissertation, a major breakthrough in CdTe-solar-cell efficiency is possible with the electron-reflector strategy.

Bibliography

[1] http://en.wikipedia.org/wiki/World_energy_resources_and_consumption

[2] http://sunearthday.nasa.gov/2007/locations/ttt_cradlegrave.php

[3] K.L. Barth, "Abound Solar's CdTe Module Manufacturing and Product Introduction", *Proc. of the 34th IEEE PVSC*, June 2009, 002264-002268.

[4] D. Rose, R. Powell, U. Jayamaha, and M. Maltby, "Advances in Performance and High-Throughput Manufacturing of Thin-Film CdS/CdTe Modules", *Proc. of the 29th IEEE PVSC*, 2002, p. 555.

[5] X. Wu, J.C. Keane, R.G. Dhere, C. DeHart, A. Duda, T.A. Gessert, S. Asher, D.H. Levi, and P. Sheldon, "16.5%-Efficient CdS/CdTe Polycrystalline Thin-Film Solar Cell", *17th European Photovoltaic Solar Energy Conference, Munich, Germany*, 22-26 October 2001, p. 995.

[6] S. M. Sze, "*Physics of Semiconductor Devices*. Second Edition.", John Wiley & Sons. 798 (1981).

[7] James Sites, Jun Pan, "Strategies to Increase CdTe Solar-Cell Voltage", *Thin Solid Films* **515** (2007) 6099–6102.

[8] R.Stangl, M.Kriegel and M. Schmidt, "AFORS-HET, Version 2.2, A Numerical Computer Program for Simulation of Heterojunction Solar Cells and Measurements", *Proc. WCPEC-4, Hawaii, USA,* May 2006, 1350-1353.

[9] M. Gloeckler, A.L. Fahrenbruch, and J.R. Sites, “Numerical Modeling of CIGS and CdTe Solar Cells: Setting The Baseline”, *Proc. World Conf. on Photovoltaic Energy Conversion 3*, 491-494 (Osaka, Japan, May 2003).

[10] Xuanzhi Wu, “High-Efficiency Polyscystalline CdTe Thin-Film Solar Cells”, *Solar Energy 77* (2004) 803-814.

[11] Alan L. Fahrenbruch, Richard H. Bube, "*Fundamentals of Solar Cells: Photovoltaic Solar Energy Conversion*", Academic Press, Inc., p. 84, 85, 281 (1983).

[12] Stephen J. Fonash, "*Solar Cell Device Physics (Energy Science and Engineering)*", Academic Press, Inc., pp. 135-137 (1981).

[13] Martin A. Green, "*Solar Cells: Operating Principles, Technology, and System Applications*", Prentice-Hall, Inc., 149(1982).

[14] J.G. Fossum, R.D. Nasby, Chong Pao Shing, "Physics Underlying The Performance of Back-Surface-Field Solar Cells", *IEEE Transactions on Electron Devices ED-27* (1980), 785-791.

[15] H.J. Hovel, “*Semiconductors and Semimetals, Vol. 11: Solar Cells*”, Academic Press, Inc., p. 23-24, 33, 52-53, 80, 96-99, 209, and 228 (1975).

[16] J. Mandelkorn and J. Lamneck, "Simplified Fabrication of Back Surface Electric Field Silicon Cells and Novel Characteristics of Such Cells", *conf. Rec. IEEE 9th PVSC,* p. 66. New York, 1972.

[17] J. G. Fossum and E. L. Burgess, "High-Efficiency p+-n-n+ Back-Surface-Field Silicon Solar Cells", *Appl. Phys. Lett*. 33, 238 (1978)

[18] Kuo-Jui Hsiao, James R. Sites, “Electron Reflector Strategy for CdTe Solar Cells”, *Proc. 34st IEEE Photovoltaics Specialists Conf., Philadelphia* (2009), pp. 001846-001850.

[19] B. Spath, J. Fritsche, F. Sauberlich, A. Klein, W. Jaegermann, “Studies of Sputtered ZnTe Films as Interlayer for The CdTe Thin Film Solar Cell”, *Thin Solid Films* 480–481 (2005) 204–207.

[20] T.L. Chu, S.S. Chu, C. Ferekides, C.Q. Wu, J. Britt, and C. Wang, "High Efficiency CdS/CdTe Solar Cells from Solution-Grown CdS Films", *Proc. of 22nd IEEE PVSC,* pp. 952-956 (1991).

[21] T. L. Chu, Shirley S. Chu, J. Britt, G. Chen, C. Ferekides, N. Schultz, C. Wang, and C. Q. Wu, "High Efficiency Thin Film Cadmium Telluride Solar Cells", *AIP Conf. Proc.* 268 88 (1992).

[22] C. Ferekides, J. Britt, Y. Ma, and L. Killian, "High Efficiency CdTe Solar Cells by Close Space Sublimation", *Proc. of 23rd IEEE PVSC,* pp. 389-393 (1993).

[23] J. Britt and C. Ferekides, "Thin-Film CdS/CdTe Solar Cell with 15.8% Efficiency", *Appl. Phys. Lett. 62,* 2851 (1993).

[24] Hideaki Ohyama, Tesuya Aamoto, Seiji Kumazawa, Hiroshi Higuhi, Takashi Arita, Satohi Shibutani, Tuyoshi Nishio, Junji Nakajima, Miwa Tsuji, Akira Hanafusa, Takeshi Hibino, Kuniyoshi Omura, and Mikio Murozono, "16.0% Efficiency Thin-Film CdS/CdTe Solar Cells", *Proc. of 26th IEEE PVSC,* pp. 343-346 (1997).

[25] V.V. Plotnikov, DoHyoung Kwon, K.A. Wieland, and A.D. Compaan, "10% Efficiency Solar Cells with 0.5 μm of CdTe", *Proc. of the 34th IEEE PVSC*, June 2009, 001435-001438.

[26] K. L. Barth and W. S. Sampath, "Environmentally Benign Vacuum Deposition with Air-to-Air Technology", *J. Mater. Res., Vol. 10, No. 3*, Mar 1995, 493-496.

[27] Barth, Kurt L., Robert A. Enzenroth and W. S. Sampath, "Advances in Continuous, In-Line Processing of Stable CdS/CdTe Devices", *29th IEEE PVSC*, May 2002, 551-554.

[28] R. A. Enzenroth, K. L. Barth, and W. S. Sampath, "Continuous In-Line Processing of CdS/CdTe Devices: Progress Towards Consistent Stability", *19th European PV Solar*

Energy Conference, June 2004, Paris, France.

[29] Barth, K. L., R. A. Enzenroth and W. S. Sampath, "Consistent Processing and Long Term Stability of CdTe Devices", *31th IEEE PVSC*, Jan. 2005, Lake Buena Vista, Florida, 323-326.

[30] R. A. Enzenroth, K. L. Barth, and W. S. Sampath, and V. Manivannan, "Performance of In-Line Manufactured CdTe Thin Film Photovoltaic Devices", *J. of Solar Energy Engineering, Vol. 129*, August 2007, 327-330.

[31] C.S. Ferekides, D. Marinskiy, V. Viswanathan, B. Tetali, V. Palekis, P. selvaraj, D.L. Morel, "High Efficiency CSS CdTe Solar Cells", *Thin Solid Films 361-362* (2000) 520-526.

[32] B.E. McCandless, L.V. Moulton, and r.W. Birkmire, "Recrystallization and Sulfur Diffusion in cdCl_2-Treated CdTe/CdS Thin Films" *Progress in Photovoltaics: Research and Applications. Vol. 5* (1997) 249-260.

[33] H.R. Moutinho, M.M. Al-Jassim, D.H. Levi, P.C. Dippo, and L.L. Kazmerski, "Effects of CdCl2 Treatment on The Recrystallization and Electro-Optical Properties of CdTe Thin Films", *J. Vac. Sci. Technol. A 16(3)*, May/Jun (1998) 1251-1257.